



저작자표시-비영리-변경금지 2.0 대한민국

이용자는 아래의 조건을 따르는 경우에 한하여 자유롭게

- 이 저작물을 복제, 배포, 전송, 전시, 공연 및 방송할 수 있습니다.

다음과 같은 조건을 따라야 합니다:



저작자표시. 귀하는 원저작자를 표시하여야 합니다.



비영리. 귀하는 이 저작물을 영리 목적으로 이용할 수 없습니다.



변경금지. 귀하는 이 저작물을 개작, 변형 또는 가공할 수 없습니다.

- 귀하는, 이 저작물의 재이용이나 배포의 경우, 이 저작물에 적용된 이용허락조건을 명확하게 나타내어야 합니다.
- 저작권자로부터 별도의 허가를 받으면 이러한 조건들은 적용되지 않습니다.

저작권법에 따른 이용자의 권리는 위의 내용에 의하여 영향을 받지 않습니다.

이것은 [이용허락규약\(Legal Code\)](#)을 이해하기 쉽게 요약한 것입니다.

[Disclaimer](#)

Thesis for the Degree of Master of Engineering

**Synthesis of Quinoxaline-based  
Conjugated Polymers with Strong  
Electron-withdrawing Cyano Group  
for Photovoltaic Application**

by

Christyowati Primi Sagita

Department of Industrial Chemistry

The Graduate School

Pukyong National University

February 2020

# **Synthesis of Quinoxaline-based Conjugated Polymers with Strong Electron-withdrawing Cyano Group for Photovoltaic Application**

(강한 전자 수용체인 시아노기를 도입한 태양전지용  
퀴녹살린 기반 전도성 고분자의 합성)

Advisor: Prof. Dong Wook Chang

by

Christyowati Primi Sagita

A thesis submitted in partial fulfillment of the requirements

for the degree of

Master of Engineering

in Department of Industrial Chemistry, The Graduate School,  
Pukyong National University

February 2020

**Synthesis of Quinoxaline-based Conjugated Polymers with  
Strong Electron-withdrawing Cyano Group for Photovoltaic  
Application**

A dissertation

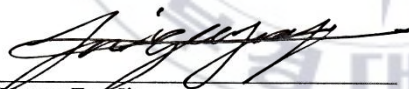
by

Christyowati Primi Sagita

Approved by:



Prof. Min Young Shon



Prof. Young Eup Jin



Prof. Dong Wook Chang

February 2020

# CONTENTS

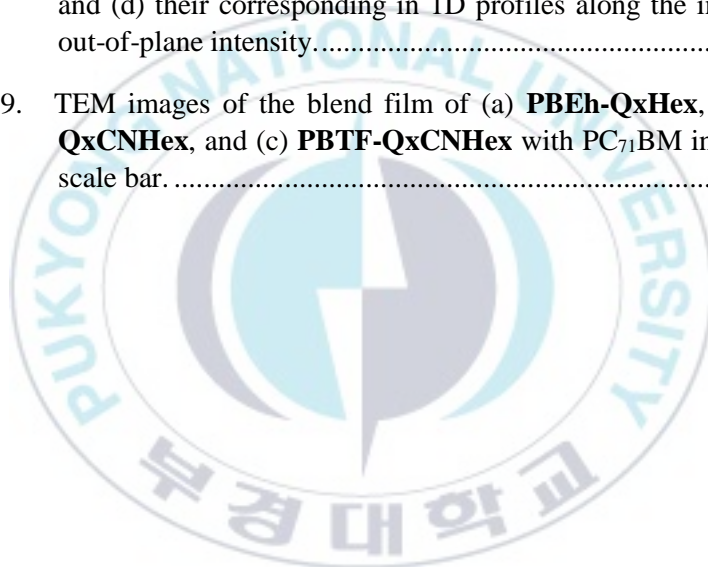
CONTENTS .....	i
List of Figures .....	iii
List of Tables.....	v
List of Schemes .....	vii
Abstract .....	viii
요약.....	viii
<b>Chapter I. Introduction.....</b>	<b>1</b>
I-1. Polymer Solar Cells.....	1
I-2. Basic Working Principles of Polymer Solar Cells.....	3
I-2.1. Light absorption and exciton generation .....	3
I-2.2. Exciton diffusion .....	4
I-2.3. Exciton dissociation.....	5
I-2.4. Charge-carrier transport and collection .....	5
I-3. Device Structure of Polymer Solar Cells.....	6
I-4. Device Parameters of Polymer Solar Cells.....	7
I-4.1. Open circuit voltage ( $V_{oc}$ ).....	8
I-4.2. Short Circuit Current Density ( $J_{sc}$ ) .....	9
I-4.3. Fill Factor ( $FF$ ).....	9
I-4.4. Incident Photon to Charge Carrier Efficiency (IPCE).....	10
I-5. Basic Principle of Molecular Engineering Design for Polymer Solar Cells .....	10
I-5.1. Low band-gap of Polymer Solar Cells.....	11
I-5.2. Polymer Backbone.....	13
I-5.3. Incorporation of electron-withdrawing groups .....	15
I-6. The Aim of Thesis .....	16

<b>Chapter II. Experimental Section .....</b>	<b>18</b>
II-1. Material and Instruments.....	18
II-2. Synthesis of Monomers.....	19
II-2.1. 1,2-bis(3-(hexyloxy)phenyl)ethane-1,2-dione (3).....	19
II-2.2. 2,3-bis(3-(hexyloxy)phenyl)-5,8-di(thiophen-2-yl)quinoxaline (5) ...	20
II-2.3. 5,8-bis(5-bromothiophen-2-yl)-2,3-bis(3-(hexyloxy)phenyl)quinoxaline (6).....	21
II-2.4. 5,8-bis(5-bromothiophen-2-yl)-2,3-bis(3-(hexyloxy)phenyl)quinoxaline-6-carbonitrile (8).....	21
II-3. General Procedure for Polymerization of BDT-dibrominated diphenyl quinoxaline by Stille-coupling reaction .....	22
II-3.1. Synthesis of PBEh-QxHex .....	23
II-3.2. Synthesis of PBEh-QxCNHex.....	24
II-3.3. Synthesis of PBTF-QxCNHex .....	24
II-4. Fabrication and analysis of photovoltaic devices.....	27
<b>Chapter III. Results and Discussion.....</b>	<b>29</b>
III-1. Synthesis and Thermal Properties of Polymers .....	29
III-2. Optical and Electrochemical Properties of Polymers .....	31
III-3. Theoretical Calculations of Polymers.....	37
III-4. Photovoltaic Properties of Polymers.....	39
<b>Chapter IV. Conclusion.....</b>	<b>50</b>
References .....	52
Acknowledgements .....	59

## List of Figures

Figure I-1.	Working principle of D-A type polymer solar cells in heterojunction structure [9].....	3
Figure I-2.	The device structure based on the normal (left) and the inverted (right) configuration with the light penetrate from the bottom of device. ITO: indium tin oxide electrode; ETL: electron transport layer; AL: active layer; HTL: hole transport layer [9].....	6
Figure I-3.	J-V curves of polymer solar cell device in the dark and under illumination [10].....	8
Figure I-4.	Hybridization of molecular orbital energy levels of D-A type polymer through delocalized $\pi$ -electron interaction in D-A interface [20].....	12
Figure I-5.	Benzodithiophene unit with various substituent [22].....	14
Figure I-6.	The structure of quinoxaline unit .....	14
Figure II-1.	Chemical structure of <b>PBEh-QxHex</b> , <b>PBEh-QxCNHex</b> , and <b>PBTF-QxCNHex</b> .....	25
Figure III-1.	TGA thermograms of <b>PBEh-QxHex</b> , <b>PBEh-QxCNHex</b> , and <b>PBTF-QxCNHex</b> at a heating rate of of 10°C/min under N <sub>2</sub> .....	31
Figure III-2.	UV-Visible spectra of polymer (a) solution in chloroform and (b) films on glass substrate (spectra are offset for clarity) .....	33
Figure III-3.	Cyclic voltammograms of polymers .....	35
Figure III-4.	Energy level diagram of all materials used in the inverted type PSCs device.....	36
Figure III-5.	Frontier molecular orbitals of two-repeating unit models with HOMO and LUMO energy levels calculated at the B3LYP/6-31G** level for (a) <b>PBEh-QxHex</b> , (b) <b>PBEh-QxCNHex</b> , and (c) <b>PBTF-QxCNHex</b> .....	41

- Figure III-6. (a) Current density vs. voltage curves of PSCs with optimum blend ratio of polymer donor to PC<sub>71</sub>BM under 1.0 sun condition (inset: under dark condition) and (b) IPCE spectra of PSCs based on **PBEh-QxHex**, **PBEh-QxCNHex**, and **PBTF-QxCNHex**. .....41
- Figure III-7. Current density vs. voltage curves of (a) hole-only and (b) electron-only devices based on **PBEh-QxHex**, **PBEh-QxCNHex**, and **PBTF-QxCNHex** including the inset showing current density vs. voltage (V) –built-in voltage (V<sub>bi</sub>) with fitted lines. ....43
- Figure III-8. GIWAXS patterns of the blend films of (a) **PBEh-QxHex**, (b) **PBEh-QxCNHex**, and (c) **PBTF-QxCNHex** with PC<sub>71</sub>BM in 2D, and (d) their corresponding in 1D profiles along the in-plane and out-of-plane intensity .....45
- Figure III-9. TEM images of the blend film of (a) **PBEh-QxHex**, (b) **PBEh-QxCNHex**, and (c) **PBTF-QxCNHex** with PC<sub>71</sub>BM in 200 nm of scale bar. ....48



## List of Tables

Table III-1.	Molecular weights of polymers .....	30
Table III-2.	Summary of optical and electrochemical properties of the polymers .....	34
Table III-3.	The best photovoltaic parameters of the PSCs. The averages for the photovoltaic parameters of each device are given in parentheses	39



## List of Schemes

Scheme 1.	Synthesis of <b>PBEh-QxHex</b> , <b>PBEh-QxCNHex</b> , and <b>PBTF-QxCNHex</b> .....	26
-----------	--	----



Synthesis of Quinoxaline-based Conjugated Polymers with Strong Electron-withdrawing  
Cyano Group for Photovoltaic Application

Christyowati Primi Sagita

Department of Industrial Chemistry, The Graduate School,  
Pukyong National University

**Abstract**

A new series of the quinoxaline-based conjugated polymers have been successfully synthesized for photovoltaic application. The polymers were synthesized by the Stille coupling reaction and have construction based on the donor- $\pi$  bridge-acceptor (D- $\pi$ -A) configuration. The 2-ethylhexyloxy benzodithiophene (BDT) as the donor backbone is connected to the di(*m*-hexyloxy) phenylquinoxaline (DPQ) acceptor backbone through thiophene bridge, to afford **PBEh-QxHex**. A cyano group, as the strong electron-withdrawing substituent, was incorporated on quinoxaline structure to yield **PBEh-QxCNHex**, since the previous studies showed that the conjugated polymers with the substituents had a notable effect on the solar cell device. The introducing of the cyano group can enhance intermolecular interaction, leading to the improvement of all photovoltaic properties. The **PBEh-QxCNHex** possesses the open-circuit voltage ( $V_{oc}$ ) of 0.79 V, short-circuit current ( $J_{sc}$ ) of 17.24 mA/cm<sup>2</sup>, and fill factor ( $FF$ ) of 53.3%. Furthermore, the substitution of 2-ethylhexyloxy to 2-ethylhexyl-fluorinated thiophene moiety on the BDT unit producing **PBTf-QxCNHex** conduces higher photovoltaic properties. These all-polymer devices were fabricated based on an inverted-type structure with ITO/ZnO/polymer: PC<sub>71</sub>BM/MoO<sub>3</sub>/Al configuration. Owing to the better planarity in **PBTf-QxCNHex**, this polymer exhibits the highest PCE of 8.66%, followed by  $V_{oc}$  of 0.92 V, short-circuit current ( $J_{sc}$ ) of 15.59 mA/cm<sup>2</sup>, and fill factor ( $FF$ ) of 60.7%.

# 강한 전자 수용체인 시아노기를 도입한 태양전지용 퀴녹살린 기반 전도성 고분자의 합성

Christyowati Primi Sagita

공업화학과, 부경대학교

## 요약

본 연구는 태양전지에 적용 가능한 새로운 퀴녹살린 기반의 공액 구조 고분자 series 를 성공적으로 합성하였다. Stille coupling reaction 을 이용하여 donor- $\pi$  bridge-acceptor (D- $\pi$ -A) 배열을 가지는 고분자를 합성하였다. 전자공여체로 사용되는 2-ethylhexyloxyn benzodithiophene(BDT)는 thiophene ring 과 연결되어 이 결합된 전자수용체의 중심인 di(m-hexyloxy)phenylquinoxaline (DPQ)와 thiophene bridge 로 연결된 구조의 고분자인 **PBEh-QxHex** 를 합성하였다. 이전의 연구에서 강한 전자 끄는 기로 알려진 cyano 기로 치환된 공액 고분자에서 상당히 좋은 태양전지 효율을 보여주었기 때문에, cyano 기가 치환된 퀴녹살린 기반 고분자 **PBEh-QxCNHex** 를 합성하였다. Cyano 기의 도입은 분자내 상호작용을 향상시킬 수 있으며, 이에 따라 태양전지의 성능을 향상시킬 수 있다. **PBEh-QxCNHex** 는 0.79 V 의 open-circuit voltage ( $V_{oc}$ ), 17.24 mA/cm<sup>2</sup> 의 short-circuit current ( $J_{sc}$ ) 그리고 53.3 %의 fill factor ( $FF$ )를 지닌다. 또한, **PBEh-QxCNHex** 의 BDT unit 에 2-ethylhexyloxy 를 대신하여 2-ethylhexyl-fluorinated thiophene 으로 치환된 BDT unit 을 이용하여 치환기로 **PBTF-QxCNHex** 을 합성하였으며, 광전자소자 성능을 향상시킬 수 있었다. 해당 고분자를 기반으로 한 소자는 ITO/ZnO/polymer: PC<sub>71</sub>BM/MoO<sub>3</sub>/Al 의 배치를 가지는 inverted-type 구조로 만들어졌다. 고분자 구조적으로 **PBTF-QxCNHex** 의 더 좋은 평면성 때문에, 해당 고분자는 0.92V 의  $V_{oc}$ , 15.59 mA/cm<sup>2</sup> 의  $J_{sc}$ , 그리고 60.7%의 fill factor 로 8.66%의 가장 좋은 소자 효율을 보였다.

# **Chapter I. Introduction**

## **I-1. Polymer Solar Cells**

Energy, with its essential role for humans alive, has been received much attention from around the world due to the global issues concerning the increasing of its demand over the past years. Regarding the prediction of fossil fuel's limited availability in the future and also the environmental impact due to the gas emission from the fuel, many efforts start moving to renewable energy resources with low impact on the environment. Nowadays, these green energy sources, such as wind, solar, hydropower, and geothermal become the primary resolution to overcome energy demand [1]. Among those, solar is interestingly considered as the most potential source to produce the cleanest energy with regards to its availability in large quantities [2].

As most widely known, solar energy in the form of light can be harvested and converted to be electricity through a semiconductor device called photovoltaic cells or solar cells. In general, the photovoltaic cells based on inorganic materials are mostly used as the primary commercial device due to their capability to produce high efficiency of device performance, currently up to 27.6% based on recent NREL 2019 research for silicon based-solar cells device [3]. However, the main problem from the photovoltaic cells based on inorganic materials is the high

fabrication cost, followed by the unfavorable impacts for environmental, related to the usage of inorganic substances.

Since this issue has been the crucial concern in the development of new technology of solar cells device to resolve energy demand lately [4,5], many further studies move the focus to develop organic photovoltaic cells owing to their promising properties such as excellent flexibility, secure processing, and low-cost on large-area device fabrication [6], in spite of their device relatively low efficiency. The recent sustain innovation in organic material synthesis and the optimization of device fabrication, in particular for polymer solar cells (PSCs) based on bulk-heterojunction (BHJ) structure, has generated much improvement of power conversion efficiencies (PCEs) to surpassed 10% [7] with fullerene-based acceptor and currently, the highest PCE of PSCs device has achieved to 16.5% with the non-fullerene acceptor [8]. Therefore, advanced research on designing and synthesizing new-conjugated polymer solar cells still need to be developed for achieving high-performance efficiency of the organic semiconductor device.

## I-2. Basic Working Principles of Polymer Solar Cells

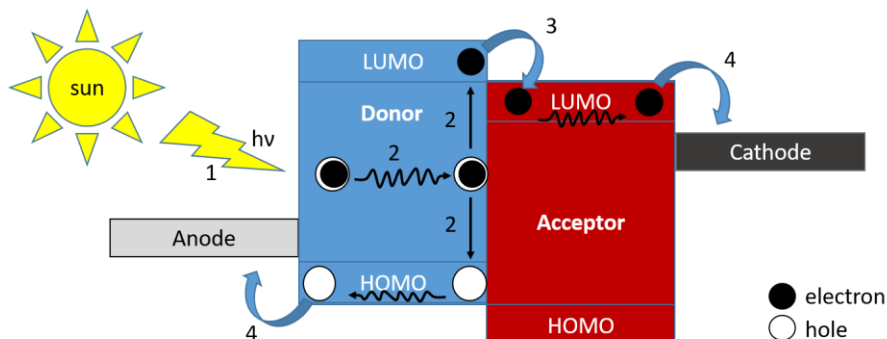


**Figure I-1.** Working principle of D-A type polymer solar cells in heterojunction structure [9]

**Figure I-1** illustrates the basic principle of the working mechanism of polymer solar cells device based on normal-type in which clarified in four steps: (1) the light absorbed in the donor layer resulted in the exciton generation; (2) the exciton diffused along the donor layer to the donor-acceptor interface, in which the exciton dissociation occurred to form a free electron and hole; (3) the separated electron then transferred from the lowest unoccupied molecular orbital (LUMO) of the donor to LUMO of the acceptor; and (4) the free-electron and free-hole collected to cathode and anode, respectively.

### I-2.1. Light absorption and exciton generation

The organic materials have a  $\pi$ - $\pi$  bond leading to the delocalized  $\pi$ -electron system, which produces a gap between LUMO and the highest occupied molecular

orbital (HOMO) called the bandgap of organic semiconducting material. As the photon absorbed in the polymer donor layer, the energy of the solar spectrum then tuned to the polymer bandgap. However, owing to the conjugated polymers have a low dielectric constant, the attraction based on coulomb forces between absorbed photon becomes very high, resulting in the generation of bound electron-hole pair called the exciton [10]. This phenomenon confirms a significant difference in organic material characteristics from inorganic one, which can directly create a free separated charge-carrier from the absorption of sunlight [11]. As a result, the generated exciton needs to separate through the next step.

### **I-2.2. Exciton diffusion**

Since the light absorption process has generated exciton, the exciton then diffuses to the interface between the donor and the acceptor. Unfortunately, the exciton has a very short lifetime, which could limit the mobility of exciton through the length of the polymer chain. Known as the exciton diffusion length, it refers to the mobility length of the exciton, which limited at the range of 10 nm. As a consequence, the decay of exciton could have occurred and inhibited the process of charge carrier separation [12]. Therefore, the selection of using heterojunction structure for solar cell devices plays a crucial role in having the possibility of effective exciton diffusion and dissociation.

### **I-2.3. Exciton dissociation**

This step occurred when the exciton has attained the interface of donor-acceptor. The dissociation relates to the separation of the exciton into free-electron and free-hole. The presence of the energy level difference between the donor LUMO and the acceptor LUMO highly provides the required energy for splitting the coupled electron-hole. The efficient dissociation of exciton could be achieved if the difference in the LUMO energy level of donor and acceptor is higher than the exciton binding energy, which is around 0.2-0.3 eV [10].

### **I-2.4. Charge-carrier transport and collection**

Related to the exciton has dissociated, the free-hole stay around in donor to be transferred to the anode while the free-electron move to acceptor to be collected at the cathode [11]. Both the free-charge carriers at respective electrode then will connect to the external circuit, and so produce electricity. During the transportation process, the interfacial recombination could be occurred, especially in hole transport, due to the lower mobility of hole charge in conducting polymer than electron mobility in acceptor material [9,11]. Therefore, the hole mobility in donor material needs improvement to have high charge transport efficiency in the thicker polymer film, to achieve better performance of PSCs device.

### I-3. Device Structure of Polymer Solar Cells

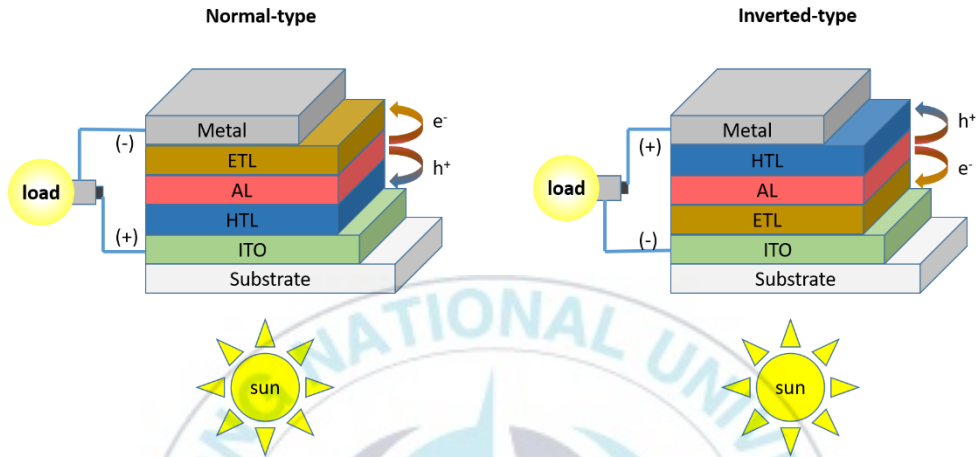


**Figure I-2.** The device structure based on the normal (left) and the inverted (right) configuration with the light penetrate from the bottom of the device. ITO: indium tin oxide electrode; ETL: electron transport layer; AL: active layer; HTL: hole transport layer [9]

Generally, there are two kinds of the device structure, that are the inverted type and the conventional or normal-type, as illustrated in **Figure I-2**. In the normal-type, the metal electrode is located on the top of the hole transporting layer, role as the hole-collected electrode. Meanwhile, the inverted has a reverse order of layer where the metal has a function as the electron-collected electrode. Also, the inverted type uses silver (Ag) as the high work-function metal, whereas the normal-type which use low work-function metal such as aluminum or calcium. Due to this significant difference in the strength of work-function metal, it proves that the

inverted type exhibits better stability to the oxygen and moisture as the device structure for photovoltaic application [13]. Currently, the bulk-heterojunction (BHJ) structure prefers to be used as active layer construction for conjugated polymers with D-A configuration than bi-layer structure. It is owing to well-known as a sandwich structure wherein the electron donor (D) blends with electron acceptor (A) unit to afford a large interfacial area of the active layer [14]. The sizeable interfacial area can have an impact on the enhancement of the performance of organic solar cells device.

#### **I-4. Device Parameters of Polymer Solar Cells**

The performance of polymer solar cells always be evaluated through power conversion efficiency (PCE) parameter, which is defined by the following formula below:

$$\text{PCE} = \frac{V_{oc} \times J_{sc} \times FF}{P_{in}}$$

wherein  $V_{oc}$  is open-circuit voltage,  $J_{sc}$  is short circuit current,  $FF$  means as fill factor, and  $P_{in}$  is incident light power density, whereas the curve shows their relationship is displayed in **Figure I-3**.

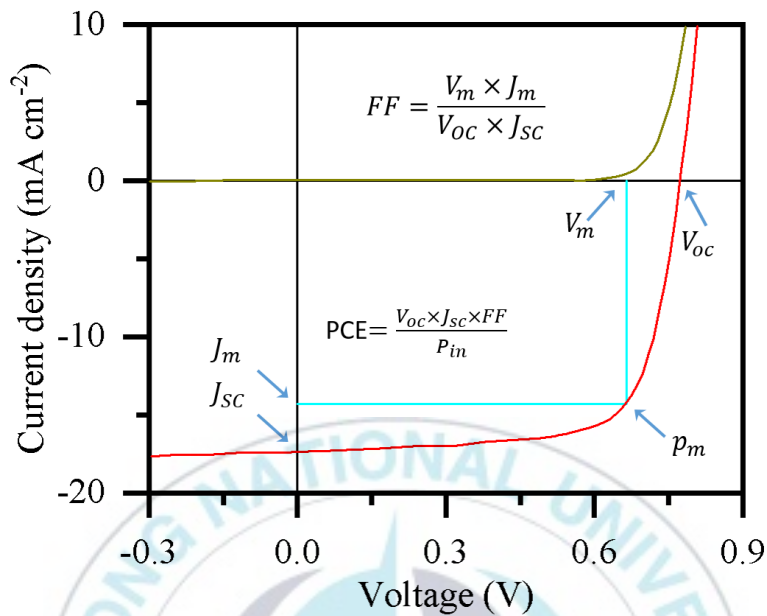


**Figure I-3.** J-V curves of polymer solar cell device in the dark and under illumination [10]

#### **I-4.1. Open circuit voltage ( $V_{oc}$ )**

The open-circuit voltage ( $V_{oc}$ ) has a definition as the maximum difference of electrical potential between two terminals in the solar cell device, where no current flows from the external circuit [9]. The value of  $V_{oc}$  correlated to the difference between the HOMO energy level of donor conjugated-polymer and the LUMO energy level of the acceptor material at the interface of donor-acceptor configuration. Presently, low-bandgap of the donor polymer offers an improvement of  $V_{oc}$  value [15], as the effort for achieving efficient exciton dissociation in the

condition the energy level offset between donor and acceptor LUMO have to be over than 0.3 V [16]. However, overmuch deep HOMO level of polymer also needs to avoid due to wider bandgap can result in reduced light absorption.

#### **I-4.2. Short Circuit Current Density ( $J_{sc}$ )**

The short-circuit current density ( $J_{sc}$ ) is described as the maximum photocurrent produced when there is no difference potential between two terminals in the solar cell device [9]. The photon flux incident of solar cells from the spectrum of the incident light is a crucial parameter to determine the  $J_{sc}$  value. Therefore, a broad and intense absorption throughout the solar spectrum region, which standardized in AM 1.5G, should be possessed by the active layer to increase the  $J_{sc}$  value [16].

#### **I-4.3. Fill Factor ( $FF$ )**

The fill factor is explained as the ratio between the maximum power produced by solar cells to the value of  $V_{oc}$  and  $J_{sc}$ . Based on the  $J$ - $V$  curve in **Figure I-3**, it will have a rectangle shape when the  $FF$  parameter achieves the ideal percentage of 100%, which determined by the formula below:

$$FF = \frac{V_m \times J_m}{V_{oc} \times J_{sc}}$$

in which  $J_m$  and  $V_m$  are the current density and the voltage at the point on the  $J$ - $V$  curve when achieving maximum output power, respectively [9]. The hole mobility and the morphology structure of the active layer can have an impact on the  $FF$  value. There are some ways to improve the interface condition of the active layer, such as adding a processing additive and use thermal and solvent annealing process [17], to achieve higher  $FF$  value.

#### **I-4.4. Incident Photon to Charge Carrier Efficiency (IPCE)**

The incident photon to current efficiency (IPCE) is the primary parameter which defines the efficient performance of photovoltaic cell device can convert light into electricity at the UV-Vis region wavelength. This parameter also describes the ratio of the number of collected carriers to the number of all incident photons on the active area of the solar cell device [18]. However, it is quite difficult to achieve ideal IPCE as 100% owing to there is a small possibility of charge recombination occurs during the exciton dissociation process, result in limitation of the IPCE value.

#### **I-5. Basic Principle of Molecular Engineering Design for Polymer Solar Cells**

Nowadays, polymer solar cell devices based on BHJ structure have advancement rapidly in achieving high-efficiency of device performance. This

performance improvement could be delivered as a result of a better understanding of molecular engineering, which consists of conjugated-polymer design and synthesis. The conjugated-polymer should have a broader absorption ability, which depends on the bandgap of energy level and has better morphology to produce excellent charge carrier mobility. Therefore, there are some strategies as the molecular engineering viewpoint to accomplish higher performance of PSCs device.

### **I-5.1. Low band-gap of Polymer Solar Cells**

The bulk-heterojunction structure, consist of a blend of electron-donating (D) and electron-accepting (A), has represented as the promising configuration for mostly conjugated polymer donors over the past years. Owing to there is the formation of intramolecular charge transfer (ICT) state in the D-A configuration, the conjugated polymer has a reduction of the bandgap leading to have a low bandgap for broader light absorption ability [19]. The further description of the hybridization of molecular orbital between D-A materials is illustrated in **Figure I-3**.

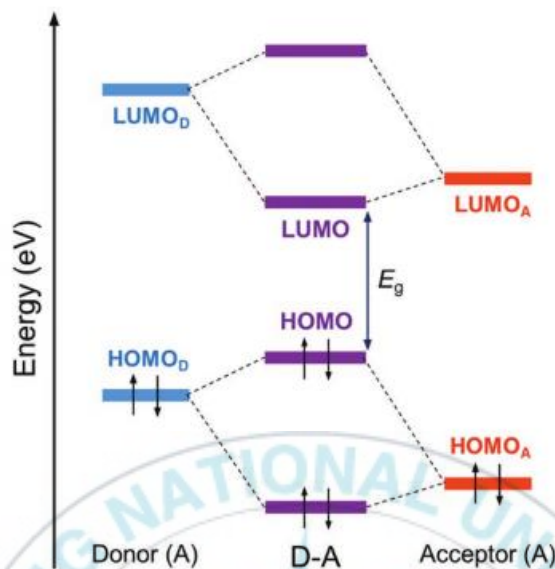


**Figure I-4.** Hybridization of molecular orbital energy levels of D-A type polymer through delocalized  $\pi$ -electron interaction in D-A interface [20]

An interaction of delocalized  $\pi$ -electron between the acceptor HOMO and the donor HOMO will form a new HOMO for the D-A interface, and so do for the interaction between the LUMO energy level in D-A polymer. Then, the strong intramolecular-interaction between new LUMO-HOMO of D-A interface through push-pull effects generate a narrow bandgap for the conjugated-polymer [20]. As reported in the previous study, a polymer solar cell with a bandgap of 1.1 eV can absorb more photon up to 77% from the solar spectrum compare to polymer solar cells which have a bandgap of 2.0 eV [21]. Hence up to now, various further studies in tuning a well-suited combination of D and A units along the polymer backbones

have been significantly developed to improve the ICT state, thus obtaining lower bandgap and preferable carrier mobility [15].

## I-5.2. Polymer Backbone

From among various of electron-donor backbone, benzodithiophene (BDT) has been well-proven as a promising electron-donating unit in conjugated polymer due to the fused aromatic structure, as shown in **Figure I-5**, which promotes high planarity and reduces the steric hindrance [22]. The fused aromatic ring with introducing two thiophene units provides better planarity and structural rigidity, which can produce beneficial interchain  $\pi$ - $\pi$  stacking [23]. However, the BDT structure needs to increase the solubility by introduction alkyl or aryl group as the side chain [24]. The high solubility toward any organic solvent gives impact to better charge carrier mobility and then improves the device parameter of the PSCs device, explained in the open-circuit voltage ( $V_{oc}$ ), short-circuit current ( $J_{sc}$ ), and fill factor ( $FF$ ) properties. The solubility also contributes to extended the  $\pi$ -conjugation length of the polymer, which results in having narrow bandgap. The presence of alkyl side chain on each side of BDT unit connected via sulfur atom reported previously enhance  $V_{oc}$  value up to 0.9 V [22]. Moreover, the planarity of the BDT unit also can be improved by introducing alkylthienyl substituent. The presence of alkyl-thiophene can enlarge the hole transport thus caused a significant improvement of PCE in PSCs device [25].

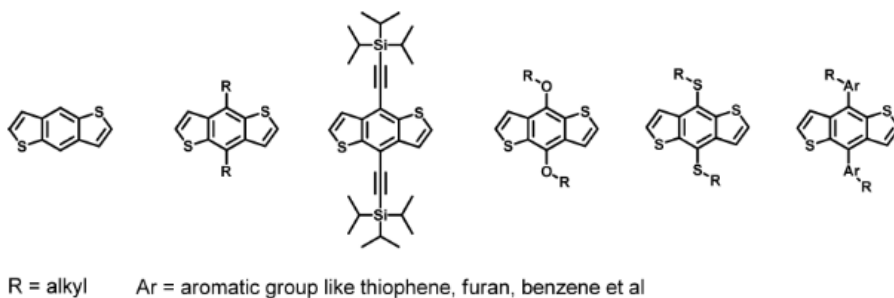


**Figure I-5.** Benzodithiophene unit with various substituent [22]

As well based on the favorable properties, quinoxaline (Qx) building block has widely known and used as a very good electron-accepting moiety owing to have superior electron affinity from the presence of two nitrogen atoms [26], illustrated in **Figure I-6**. The quinoxaline derivatives are also simple for preparation and ease of modification to have better photovoltaic characteristics [27]. Incorporation of various substituents, such as side chain, aromatic ring, and electron-withdrawing group to 2, 3, 6, and 7 positions of the quinoxaline can tune the optical-electrochemical properties and give enhancement of performance device efficiency [28].

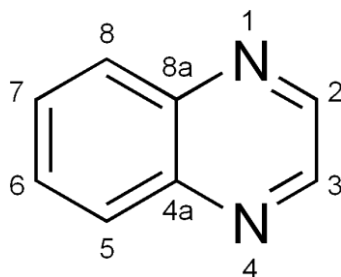


**Figure I-6.** The structure of quinoxaline unit

Putri et al. reported a PCE enhancement of PSCs device with the introduction of fluorine atoms and the trifluoromethyl group on the quinoxaline structure [29,30]. The other studies also demonstrate the valuable impact of the introducing side chain in a different position on the quinoxaline unit. A stronger intermolecular interaction through  $\pi$ - $\pi$  stacking was introduced in polymer with meta than para position, causing to enhance  $V_{oc}$  value and thus improved the PCE of device [31].

### **I-5.3. Incorporation of electron-withdrawing groups**

The introduction of various substituents in the conjugated polymer structure, especially attached in the acceptor unit, has revealed a notable effect on optical and electrochemical properties such as lowering HOMO energy level [30,32-33]. Since the alkyl side chain is contributing as the electron-rich substituent, the incorporation of electron-drawing substituent needed to control the bandgap of the conjugated polymer and also improve the crystallinity and morphology structure for better photovoltaic device performance. In particular, the cyano group (-CN) has known to have a superior dipole moment, which supports charge separation efficiently in BHJ conjugated polymer structure [34]. The CN substituent can lower both the lowest unoccupied molecular orbital (LUMO) and the highest occupied molecular orbital (HOMO) energy levels, resulting in higher  $V_{oc}$  value, and so do the conversion efficiency of the PSCs device compare with polymer

without cyano group [34,35]. The cyanated-conjugated polymer also shows excellent stability thermal for semiconducting material applications [36]. However, increasing the number of the cyano group observed to have a reduction in the PSCs device performance. As informed by Lu et al., the PCE of polymer with two cyano groups has decreased from 4.21% to 0.03%, and likewise, Casey et al. demonstrated the smallest PCE of 0.63% from two-CN polymer compare to the one-CN polymer [34,37]. Unfortunately, the study to concern the effect a cyano substituent in quinoxaline conjugated-polymer is still limited and needs further investigation [38]. Apart from the acceptor unit, incorporation of electron-withdrawing moiety on the donor unit nowadays has attracted significant interest, particularly with a fluorine atom [39]. According to its ability to exhibit lower HOMO and LUMO energy levels as well as control the aggregation in morphology structure, the fluorinated-BDT unit results in improved device performance [40].

## **I-6. The Aim of the Thesis**

This thesis aims to obtain further insight and understanding in designing and synthesizing three new of the D-A type-conjugated polymers based on quinoxaline backbone with introducing the cyano group as the electron-withdrawing for photovoltaic cell application. In this series polymers with the D-A configuration, benzodithiophene (BDT) used as the electron-donating unit, while 2,3-

diphenylquinoxaline (DPQ) as the electron-accepting unit. A cyano group was introduced to the 6-position of the quinoxaline, and hexyl side chain was incorporated in meta position of the phenyl ring at 2,3-position of DPQ. Besides, a fluorine atom was introduced in alkythienyl group on BDT unit to produce the third polymer.



## Chapter II. Experimental Section

### II-1. Material and Instruments

1-bromo-3-(hexyloxy)benzene (2), 4,7-di(thiophen-2-yl)benzo[c][1,2,5]thiadiazole (4), and 4,7-bis(5-bromothiophen-2-yl)benzo[c][1,2,5]thiadiazole-5-carbonitrile (7) were synthesized according to the previously reported procedures [34,41-42]. For 4,8-bis((2-ethylhexyl)oxy)benzo[1,2-b:4,5-b']dithiophene-2,6-diylbis(trimethylstannane) (9) and 4,8-bis(2-ethylhexyl)-4-fluorothiophen-2-yl benzo[1,2-b:4,5-b']dithiophene-2,6-diylbis(trimethylstannane) (10) were purchased from Derthon Optoelectronic Materials Science Technology Co., Ltd., meanwhile all other chemicals and solvents were obtained from Sigma-Aldrich Co., Inc. All of nuclear magnetic resonance spectra for  $^1\text{H}$ ,  $^{13}\text{C}$ , and  $^{19}\text{F}$  were measured with a JEOL JNM-ECA-600 spectrometer. UV Visible spectra was carried out in JASCO V-530 UV-Vis spectrometer. A Bruker Ultraflex spectrometer was used for Matrix-assisted laser desorption/ionization time-of-flight (MALDI-TOF) measurement. Gel Permeation Chromatography was analysed in THF solvent by using Agilent 1200 series instrument. A VersaSTAT3 potentiostat (Princeton Applied Research) with 0.1 M tetrabutylammonium hexafluorophosphate solution ( $\text{Bu}_4\text{NPF}_6$ ) in acetonitrile as the electrolyte was used for cyclic voltammetry (CV) analysis. Furthermore, in CV measurement, a glassy carbon electrode was used as a working electrode with a

coated sample of polymers on it meanwhile, the counter electrode was used a platinum wire and silver wire was used for pseudo-reference electrode with a ferrocene/ferrocenium as the external standard.

## II-2. Synthesis of Monomers

### II-2.1. 1,2-bis(3-(hexyloxy)phenyl)ethane-1,2-dione (3)

In a two-neck round bottom flask, 1-bromo-3(hexyloxy)benzene (**2**, 11.7 mmol) in 60 ml THF under nitrogen protection was stirred at  $-78^{\circ}\text{C}$  for 30 minutes. After that, n-butyllithium (2.5 M solution in Hexane, 4.7 mL) was added dropwise slowly into the cold solution and continued to stir for another 1 hr. The mixture solution of reaction then was added by 1,4-dimethylpiperazine (5.30 mmol) as soon as possible, still at the low temperature, and just let stirred once more for 1 hr. After 1 hr, the solution was moved to room temperature to be warm for overnight. A 50 ml of 10% HCl solution later was added to the mixture solution, stirred for 1 hr and then followed by the extraction with ethyl acetate. The solvent was removed in vacuum condition and column chromatography was done to purify the product using ethyl acetate/hexane (1/20, v/v) as the eluent. Yield = 86% (yellow liquid).  $^1\text{H}$  NMR (600 MHz,  $\text{CDCl}_3$ ):  $\delta$  (ppm) = 7.51 (m, 2H), 7.45 (d, 2H,  $J = 8.04$  Hz), 7.39-7.37 (t, 2H,  $J = 8.04$  Hz), 7.20-7.17 (m, 2H), 4.00 (t, 4H,  $J = 6.54$  Hz), 1.82-1.76 (m, 4H), 1.49-1.43 (m, 4H), 1.38-1.31 (m, 8H), 0.91 (t, 6H,  $J = 7.08$  Hz).  $^{13}\text{C}$

NMR (150 MHz, CDCl<sub>3</sub>): 194.2, 159.5, 134.1, 129.8, 122.6, 121.7, 113.6, 68.1, 31.4, 28.9, 25.5, 22.4, 13.8. MALDI-TOF MS: m/z calcd, 410.246; found, 410.224 [M<sup>+</sup>].

## **II-2.2. 2,3-bis(3-(hexyloxy)phenyl)-5,8-di(thiophen-2-yl)quinoxaline (5)**

Into a solution of 4,7-di(thiophen-2-yl)benzo[c][1,2,5]thiadiazole (**4**, 1 mmol) in 30 ml of acetic acid was added zinc powder (20 mmol) and stirred for 12 hr at 80°C until the color was changed to be white. After the reaction was completed, the zinc powder was directly filtered whereas into the filtrate was added 1,2-bis(3-(hexyloxy) phenyl)ethane-1,2-dione (**3**, 1 mmol) and continued to stir at reflux temperature for overnight. Upon cooling down to room temperature, the solid was formed and collected by filtration. The solid was washed by methanol and the solvent then was removed in vacuum condition. The product was purified by column chromatography using dichloromethane/hexane (1/2, v/v) as the eluent. Yield = 45% (yellow solid). <sup>1</sup>H NMR (600 MHz, DMSO): δ (ppm) = 8.41 (s, 2H), 8.06 (dd, 2H, *J* = 4.02, 1.02 Hz), 7.75 (dd, 2H, *J* = 5.31, 1.50 Hz), 7.34 (t, 2H, *J* = 8.04 Hz), 7.26-7.23 (m, 6H), 7.00-6.98 (m, 2H), 3.89 (t, 4H, *J* = 6.54 Hz), 1.67-1.62 (m, 4H), 1.39-1.34 (m, 4H), 1.32-1.27 (m, 8H), 0.90-0.87 (m, 6H). <sup>13</sup>C NMR (150 MHz, CDCl<sub>3</sub>): 158.9, 151.3, 139.8, 138.5, 136.9, 131.0, 129.0, 128.6, 126.8, 126.5, 126.2, 122.8, 116.4, 115.6, 68.0, 31.5, 29.1, 25.7, 22.6, 14.0. MALDI-TOF MS: m/z calcd, 646.904 ; found, 647.337 [M<sup>+</sup>].

### **II-2.3. 5,8-bis(5-bromothiophen-2-yl)-2,3-bis(3-(hexyloxy)phenyl)quinoxaline (6)**

A *N*-Bromosuccinimide (1.32 mmol) was added into solution of 2,3-bis(3-(hexyloxy)phenyl)-5,8-di(thiophen-2-yl)quinoxaline (**5**, 0.6 mmol) in 20 mL of dry THF. The mixture was stirred for 12 hr at room temperature. Afterwards, the mixture was poured into water and extracted using ethyl acetate. The organic phase was dried over MgSO<sub>4</sub> and the solvent was removed under vacuum pressure. Column chromatography using ethyl acetate/hexane (1.5, v/v) as the eluent, was done to purify the product. Yield = 68% (yellow-orange solid). <sup>1</sup>H NMR (600 MHz, CDCl<sub>3</sub>): δ (ppm) = 8.11(s, 2H), 7.57 (d, 2H, *J* = 4.02 Hz), 7.55 (t, 2H, *J* = 2.52 Hz), 7.22 (t, 2H, *J* = 8.04 Hz), 7.13 (d, 2H, *J* = 4.02 Hz), 7.12 (d, 2H, *J* = 7.56 Hz), 6.99-6.97 (m, 2H), 4.05 (t, 4H, *J* = 6.54 Hz), 1.83-1.78 (m, 4H), 1.52-1.47 (m, 4H), 1.38-1.33 (m, 8H), 0.93-0.91 (m, 6H). <sup>13</sup>C NMR (150 MHz, CDCl<sub>3</sub>): 159.3, 151.3, 139.3, 139.0, 135.8, 129.8, 128.8, 128.7, 124.9, 122.9, 117.2, 117.1, 114.9, 68.3, 31.7, 29.3, 25.9, 22.7, 14.1. MALDI-TOF MS: *m/z* calcd, 804.696; found, 805.213 [M<sup>+</sup>].

### **II-2.4. 5,8-bis(5-bromothiophen-2-yl)-2,3-bis(3-(hexyloxy)phenyl)quinoxaline-6-carbonitrile (8)**

Into a solution of 4,7-di(thiophen-2-yl)benzo[*c*][1,2,5]thiadiazole (**4**, 0.62 mmol) in 12 ml of acetic acid was added zinc powder (12.42 mmol) and stirred for 45 min at 80°C until the color was changed to be white. Then, the zinc powder was

directly filtered whereas into the filtrate was added 1,2-bis(3-(hexyloxy)phenyl)ethane-1,2-dione (**3**, 0.62 mmol) and continued to stir at reflux temperature for overnight. After cooling down to room temperature, the solid was formed and collected by filtration. The solid was washed by methanol and the solvent then was removed in vacuum condition. The product was purified by column chromatography using dichloromethane/hexane (1/3, v/v) as the eluent. Yield = 58.8% (orange solid). <sup>1</sup>H NMR (600 MHz, CDCl<sub>3</sub>): δ (ppm) = 8.28 (s, 1H), 7.92 (d, 1H, *J* = 4.02 Hz), 7.60 (d, 1H, *J* = 4.02 Hz), 7.55 (s, 1H), 7.50 (s, 1H), 7.25-7.19 (m, 3H), 7.18 (d, 1H, *J* = 4.08 Hz), 7.13 (d, 1H, *J* = 7.56 Hz), 7.08 (d, 1H, *J* = 7.56 Hz), 7.01 (dd, 1H, *J* = 8.04, 2.52 Hz), 6.99 (dd, 1H, *J* = 8.04, 2.52 Hz), 4.06-4.00 (m, 4H), 1.84-1.76 (m, 4H), 1.53-1.46 (m, 4H), 1.38-1.32 (m, 8H), 0.92 (t, 6H, *J* = 6.54 Hz). <sup>13</sup>C NMR (150 MHz, CDCl<sub>3</sub>): 159.4, 153.5, 153.1, 138.4, 138.3, 137.3, 137.1, 136.5, 135.2, 134.0, 131.0, 130.4, 129.3, 129.2, 129.1, 128.2, 126.4, 122.9, 122.8, 120.1, 119.0, 118.8, 118.0, 117.7, 115.0, 114.9, 109.1, 68.3, 31.6, 29.3, 25.8, 22.6, 14.1. MALDI-TOF MS: *m/z* calcd, 827.100; found, 827.085 [M<sup>+</sup>].

### II-3. General Procedure for Polymerization by Stille-coupling reaction

A mixture of BDT monomer (0.19 mmol), dibrominated-DPQ monomer (**6**, **8**; 0.19 mmol) and Pd(PPh<sub>3</sub>)<sub>4</sub> (3% mol) was dissolved in 10 ml toluene under nitrogen bubbling for 15 min, in a Schlenk flask. Then, the solution was moved to

the temperature of 90°C and stirred for 48 days with nitrogen protection. Two of end-capping agents (2-trimethylstannylthiophene and 2-bromothiophene) were sequentially added at 2 hr interval to end the polymerization reaction. Afterward, the solution was precipitated in methanol and the solid was continued to be filtered. The polymer solid was further purified by using soxhlet extraction with solvents methanol, acetone, hexane and chloroform, sequentially. After the polymer was all dissolved in chloroform, the solvent was removed partially under vacuum condition to afford concentrated polymer solution which then precipitated one more time in methanol. The purified polymer solid was filtered and dried overnight at 50°C under vacuum pressure.

### II-3.1. Synthesis of PBEh-QxHex

4,8-bis((2-ethylhexyl)oxy) benzo[1,2-b:4,5-b'] dithiophene-2,6-diyl)bis(trimethylstannane) (**9**) and dibrominated-DPQ monomer (**6**) were used as the reactant. Yield = 93.3% (deep blue solid). <sup>1</sup>H NMR (600 MHz, CDCl<sub>3</sub>): δ (ppm) = 7.86-7.52 (br, 2H), 7.52-7.39 (br, 2H), 7.39-7.28 (br, 2H), 7.24-7.15 (br, 2H), 7.15-7.07 (br, 2H), 7.07-6.89 (br, 4H), 6.89-6.73 (br, 2H), 4.39-3.21 (br, 8H), 1.73-1.62 (br, 6H), 1.52-1.14 (br, 28H), 1.12-0.80 (br, 18H). Molecular weight by GPC: number-average molecular weight (M<sub>n</sub>) = 103.44 KDa, polydispersity index (PDI) = 2.43. Elemental analysis: calcd (%) for C<sub>66</sub>H<sub>76</sub>N<sub>2</sub>O<sub>4</sub>S<sub>4</sub> : C 72.75, H 7.03, N 2.57, S 11.77; found: C 73.38, H 7.10, N 2.55, S 13.86.

### II-3.2. Synthesis of PBEh-Q<sub>x</sub>CNHex

4,8-bis((2-ethylhexyl) oxy) benzo[1,2-b:4,5-b'] dithiophene-2,6-diyl) bis(trimethylstannane) (**9**) and dibrominated-DPQ monomer (**8**) were used as the reactant. Yield = 87.7% (deep green solid). <sup>1</sup>H NMR (600 MHz, CDCl<sub>3</sub>): δ (ppm) = 8.44-8.04 (br, 1H), 8.04-7.68 (br, 2H), 7.69-7.49 (br, 2H), 7.46-7.24 (br, 4H), 7.18-7.12 (br, 1H), 7.12-6.94 (br, 3H), 6.94-6.86 (br, 1H), 6.86-6.54 (br, 1H), 4.52-3.27 (br, 8H), 1.96-1.74 (br, 6H), 1.40-1.08 (br, 28H), 1.06-0.78 (br, 18H). Molecular weight by GPC: number-average molecular weight (M<sub>n</sub>) = 102.12 KDa, polydispersity index (PDI) = 3.69. Elemental analysis: calcd (%) for C<sub>67</sub>H<sub>75</sub>N<sub>3</sub>O<sub>4</sub>S<sub>4</sub>: C 72.20, H 6.78, N 3.77, S 11.51; found: C 72.56, H 6.89, N 3.54, S 11.45.

### II-3.3. Synthesis of PBTF-Q<sub>x</sub>CNHex

4,8-bis(5-(2-ethylhexyl)-4-fluorothiophen-2-yl) benzo[1,2-b:4,5-b'] dithiophene-2,6-diyl) bis(trimethylstannane) (**10**) and dibrominated-DPQ monomer (**8**) were used as the reactant. Yield = 93.6% (deep green solid). <sup>1</sup>H NMR (600 MHz, CDCl<sub>3</sub>): δ (ppm) = 8.58-8.32 (br, 1H), 8.08-7.82 (br, 2H), 7.60-7.37 (br, 6H), 7.37-7.26 (br, 1H), 7.26-7.16 (br, 2H), 7.07-6.99 (br, 2H), 6.87-6.42 (br, 3H), 4.12-2.66 (br, 8H), 2.03-1.93 (br, 4H), 1.90-1.50 (br, 22H), 1.44-1.39 (br, 9H), 1.24-1.08 (br, 10H), 1.05-0.97 (br, 7H). Molecular weight by GPC: number-average molecular weight (M<sub>n</sub>) = 64.77 KDa, polydispersity index (PDI) = 4.38.

Elemental analysis: calcd (%) for  $C_{75}H_{77}F_2N_3O_2S_6$ : C 70.11, H 6.20, N 3.27, S 14.97; found: C 69.58, H 6.21, N 3.16, S 16.86.

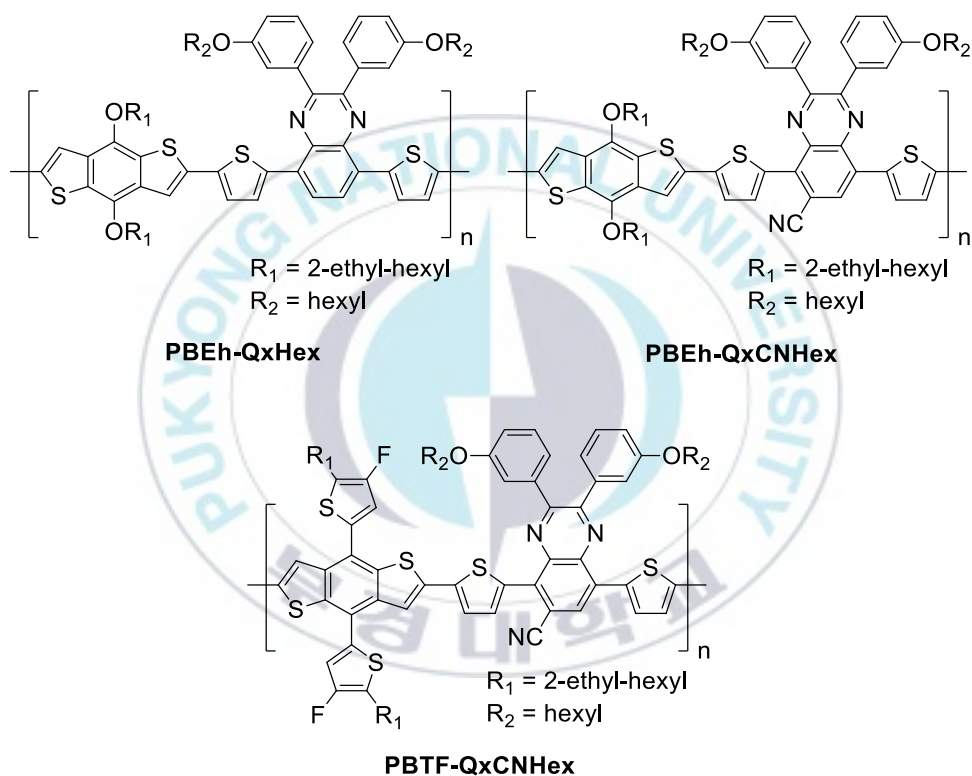
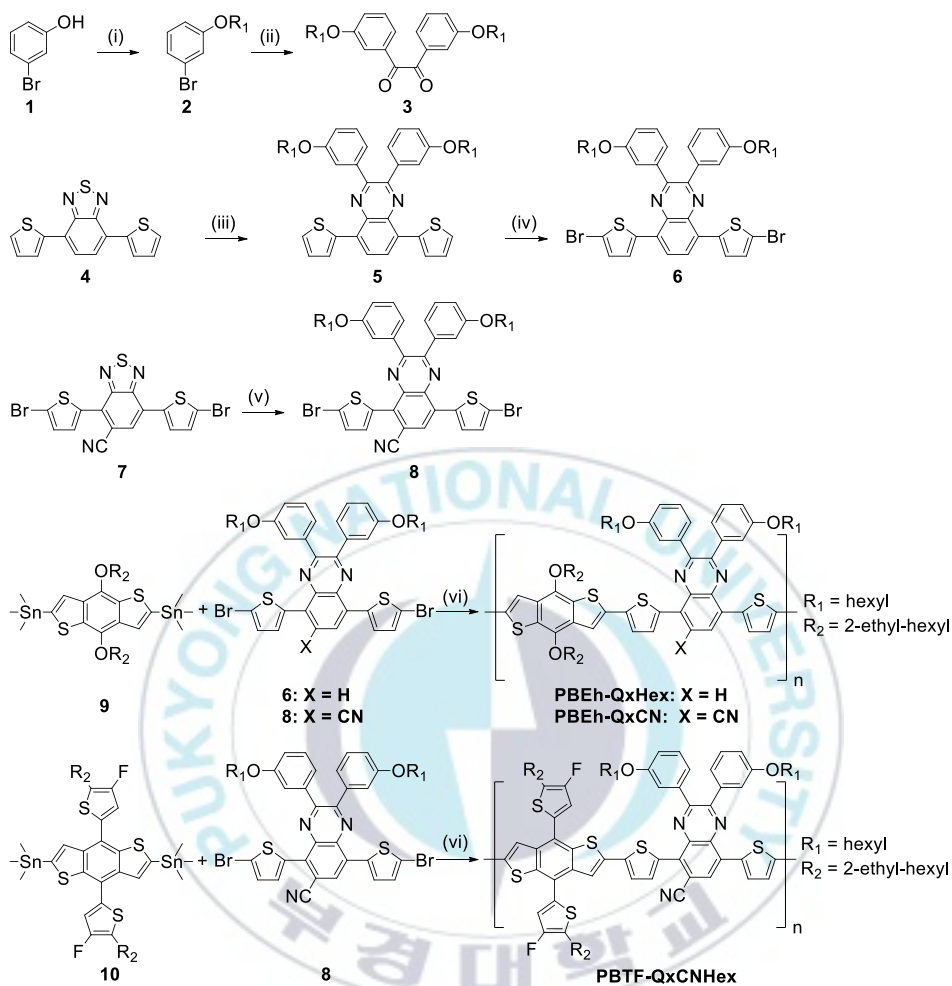


**Figure II-1.** Chemical structure of **PBEh-QxHex**, **PBEh-QxCNHex**, and **PBTF-QxCNHex**



**Scheme 1.** Synthesis of **PBEh-QxHex**, **PBEh-QxCNHex**, and **PBTF-QxCNHex**. (i) 1-bromohexane,  $K_2CO_3$ , DMF,  $100^\circ C$ , overnight; (ii) *n*-Butyllithium (2.5M), THF,  $-78^\circ C$ , 1 h; 1,4-dimethylpiperazine-2,3-dione,  $-78^\circ C$ , 1 h; then RT, overnight; (iii) zinc, acetic acid,  $80^\circ C$ , 12 h; then  $\alpha$ -diketone (**3**), reflux, 12 h; (iv) *N*-Bromosuccinimide, THF, RT, 12 h; (v) zinc, acetic acid,  $80^\circ C$ , 45 min; then  $\alpha$ -diketone (**3**), reflux, 12 h; (vi)  $Pd(PPh_3)_4$ , toluene,  $90^\circ C$ , 48 h.

## II-4. Fabrication and analysis of photovoltaic devices

The inverted-type of the polymer solar cells device has fabricated with ITO/ZnO/active layer/MoO<sub>3</sub>/Ag structure in which the active layer used is the blending of the donor polymer and PC<sub>71</sub>BM. The purchased of [6,6]-Phenyl C<sub>71</sub> butyric acid methyl ester (PC<sub>71</sub>BM, Catalog No. nano-cPCBM-SF) was from nano-C, Inc. The fabrication started with the preparation of the sol-gel process to produce ZnO film with a thickness of 25 nm, then deposited on ITO glass. At first, zinc acetate dihydrate (0.164 g) mixed with ethanolamine (0.05 mL) in 1 mL of methoxyethanol at 60°C for 30 min, after that continued with the thermal curing at 200°C for 10 min to crystallize ZnO film in partial. In the subsequent step, to prepare the active layer from the blend solution, 6 mg of polymer and 10 mg of PC<sub>71</sub>BM dissolved in 1 mL of chlorobenzene with the addition of 3% v/v 1,8-diiodooctane (DIO), and followed by the filtration using 0.2 μm polytetrafluoroethylene membrane filter. The blend solution then formed the active layer with a thickness of 95 nm by using spin coating at 1800 rpm for 120 s, the film was measured by Alpha-Step IQ surface profiler (KLA-Tencor Co.). The next step MoO<sub>3</sub> and Ag with a thickness of 3 nm and 100 nm, respectively, were sequentially coated on the top of the active layer. As the last step, the thermal evaporation via a shadow mask with a device area of 0.13 cm<sup>2</sup> at 2 x 10<sup>-6</sup> Torr was done to complete the fabrication. A KEITHLEY Model 400 source-measure unit under the 1.0 sun (100 mW/cm<sup>2</sup>) condition from 150 W Xe lamp with AM

1.5G filter was used to measure the J-V characteristic of the device by the calibration simulation condition using a Silicon (Si) reference with a certified KG5 filter from National Institute of Advanced Industrial Science and Technology.



## Chapter III. Results and Discussion

### III-1. Synthesis and Thermal Properties of Polymers

The synthetic routes to prepare all monomers and polymers are illustrated in **Scheme 1**. For the monomers, the synthesis was started from preparation of compound **3**. This compound was first prepared with alkylation of compound **1** to afford compound **2**, then continued by the next reaction using dimethylpiperazine-2,3-dione as the reactant. To produce compound **5** and **8**, the reduction of compound **4** and **7** were done using zinc powder and followed by condensation with compound **3** as the  $\alpha$ -diketone. Bromination with *N*-Bromosuccinimide (NBS), as the final step, was done to afford the final monomer of compound **6** meanwhile compound **8** can be used directly for polymerization. The benzodithiophene (BDT) monomers were used as the electron-donating with 2-ethylhexyloxy chain (compound **9**) whereas, on the compound **10** the alkoxy substituent was changed to alkylthienyl group in the order to promote planarity of structure. Finally, all of conjugated polymers with D- $\pi$ -A configuration were synthesized between the relevant DPQ monomers (compound **6** and **8**) and the BDT monomers (compound **9** and **10**) under Stille coupling condition producing **PBEh-QxHex**, **PBEh-QxCNHex**, and **PBTF-QxCNHex**, successively, as shown in **Figure II-1**, with high yields. The chemical structure of all synthesized materials had been clearly confirmed by various analytical techniques. All polymers were well soluble in

common organic solvents such as THF, chloroform, and toluene owing to the presence of alkyl chain in both BDT and DPQ monomers.

**Table III-1.** Molecular weights of polymers

<b>Polymer</b>	<b>M<sub>n</sub> (kDa)</b>	<b>M<sub>w</sub> (kDa)</b>	<b>PDI</b>
<b>PBEh-QxHex</b>	103.44	251.68	2.43
<b>PBEh-QxCNHex</b>	102.12	376.94	3.69
<b>PBTF-QxCNHex</b>	64.77	284.17	4.38

The number-average molecular weights ( $M_n$ ), weight-average molecular weights ( $M_w$ ) and polydispersity index (PDI) values of all polymers, which were obtained by gel permeation chromatography, are relatively high shown in **Table III-1**. The  $M_n$  and PDI values of three polymers vary in the range from 64.77 to 103.44 and from 2.43 to 4.38, respectively. As shown in **Figure III-1**, all polymers display good thermal stability, as measured by thermogravimetric analysis (TGA) at a heating rate of 10°C/min under nitrogen atmosphere. This thermal stability is proven with high onset decomposition temperature at 5% weight loss ( $T_{d5\%}$ ) for **PBEh-QxHex**, **PBEh-QxCNHex**, and **PBTF-QxCNHex**, in which are 340°C, 319°C, and 421°C, respectively.

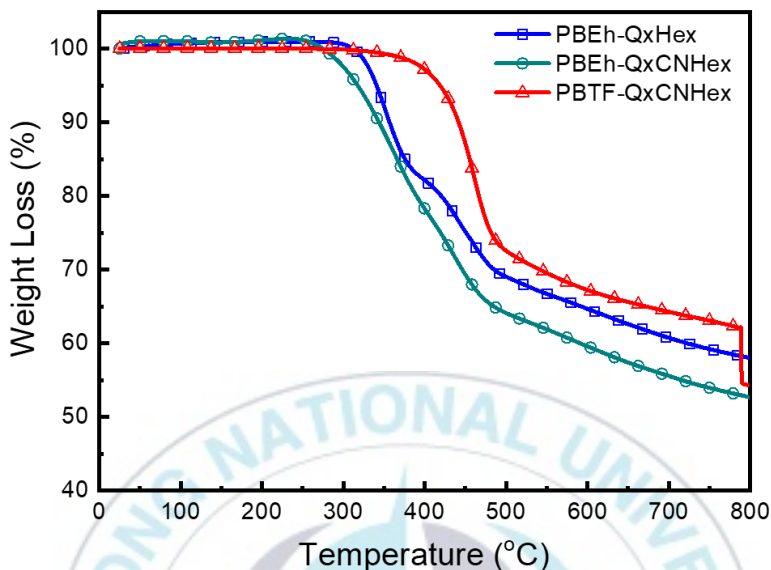


**Figure III-1.** TGA thermograms of **PBEh-QxHex**, **PBEh-QxCNHex**, and **PBTF-QxCNHex** at a heating rate of of 10°C/min under N<sub>2</sub>

### III-2. Optical and Electrochemical Properties of Polymers

To investigate the optical properties of all polymers, the UV-Vis absorption spectra both in solution and thin-film state have been measured, as illustrated in **Figure III-2a,b**, and show two broad absorption peaks at a UV-Visible wavelength range of 350-490 and 500-780 nm for shorter and longer wavelength region, respectively. The band at shorter wavelength refers to localized of  $\pi$ - $\pi^*$  transition of the polymer chains whereas the band at longer one relates to intramolecular

charge transfer (ICT) between the donor-acceptor units owing to D-A configuration in the polymer backbone. As listed in **Table III-2** and also shown in **Figure III-2a,b**, there is a shift of absorption band to the longer wavelength in the polymer film compare to in solution state for all polymers. This shift possibly attributes to an extended conjugation length of the polymer chain owing to a stronger intermolecular interaction in the solid-state [29,43], which also supported by the presence of alkyl side chain on quinoxaline structure in the meta position [31].

According to **Table III-2**, the maximum absorption in the weaker energy region of **PBEh-QxHex**, **PBEh-QxCNHex**, and **PBTF-QxCNHex** film are 604, 637, and 645 nm, respectively. The absorption band of **PBEh-QxCNHex** is red-shifted than **PBEh-QxHex** in consequence of adding cyano group into the quinoxaline backbone. The incorporation of one cyano group which have a higher electron-withdrawing ability, result in increasing of the ability of absorption light at the longer wavelength, as reported by the previous results [34,44]. Similar red-shift also occurs in the absorption maxima of **PBTF-QxCNHex** in comparison to **PBEh-QxCNHex** owing to substitution of alkoxy to alkylthienyl group with fluorination on BDT unit which gives excellent conjugation length of **PBTF-QxCNHex** [29]. The changes in absorption maximum spectra can be interpreted into decreased of the optical band gaps, calculated from the absorption edge polymer films, which are 1.71, 1.66 and 1.65 eV for **PBEh-QxHex**, **PBEh-QxCN-**

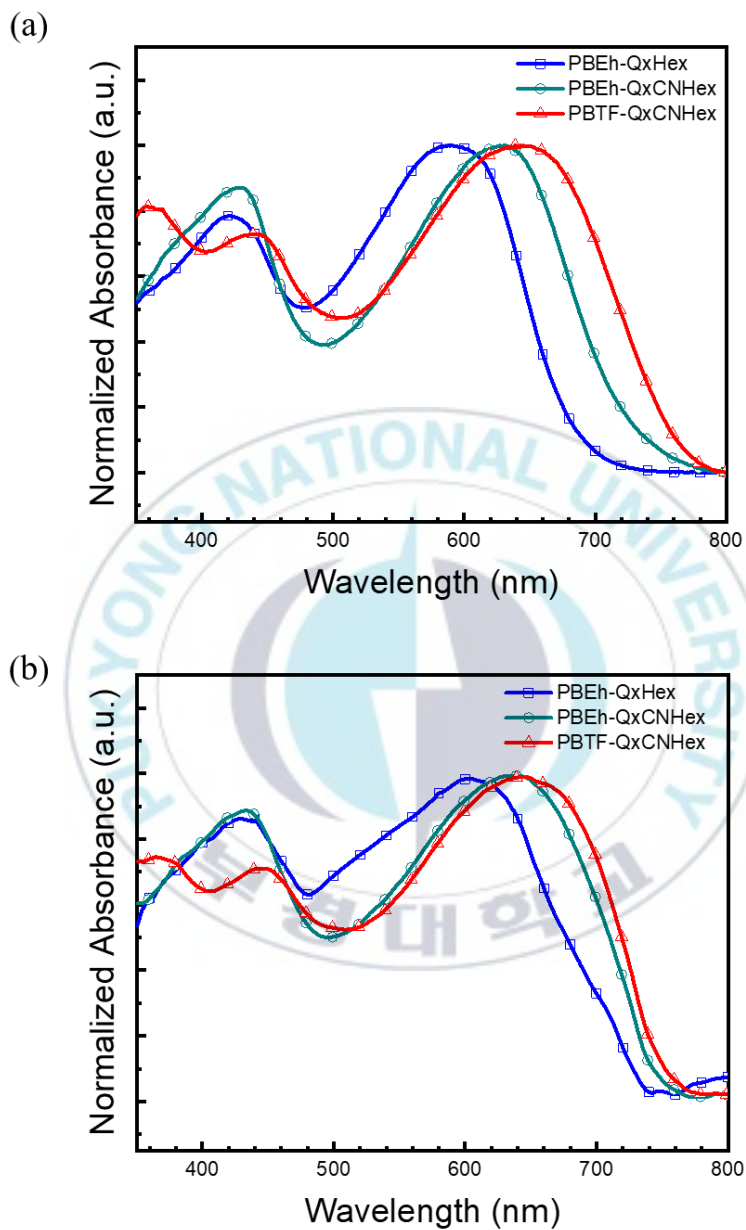


**Figure III-2.** UV-Visible spectra of polymer (a) solution in chloroform and (b) films on glass substrate (spectra are offset for clarity)

**Table III-2.** Summary of optical and electrochemical properties of the polymers

Polymer	$\lambda_{\text{edge}}$ (nm) <sup>a</sup> , $E_{\text{gap}}^{\text{opt}}$ (eV) <sup>b</sup>	$\lambda_{\text{max}}^{\text{soln}}$ (nm) <sup>c</sup> $(\lambda_{\text{max}}^{\text{film}})$ (nm) <sup>d</sup>	HOMO (eV) <sup>e</sup>	LUMO (eV) <sup>f</sup>
<b>PBEh-QxHex</b>	725, 1.71	590 (604)	-5.04	-3.33
<b>PBEh-QxCNHex</b>	749, 1.66	631 (637)	-5.17	-3.51
<b>PBTF-QxCNHex</b>	751, 1.65	639 (645)	-5.25	-3.60

<sup>a</sup>Absorption edge of the film, <sup>b</sup>Estimated bandgap from the  $\lambda_{\text{edge}}$ , <sup>c</sup>Maximum wavelength of the polymer solution in CHCl<sub>3</sub>, <sup>d</sup>Maximum wavelength of the film, <sup>e</sup>Estimated from the oxidation onset potential, <sup>f</sup>Calculated from the optical band gap and the HOMO energy level.

**Hex**, and **PBTF-QxCNHex**, respectively. The significant reduction of the optical bandgap from **PBEh-QxHex** to **PBEh-QxCNHex** occurred due to the presence of one cyano group which increase the electron deficiency of the group which increase the electron deficiency of the acceptor unit [34] meanwhile a slight decrease from **PBEh-QxCNHex** to **PBTF-QxCNHex** is caused by a little effect from the incorporation of fluorine on BDT donor unit [40].

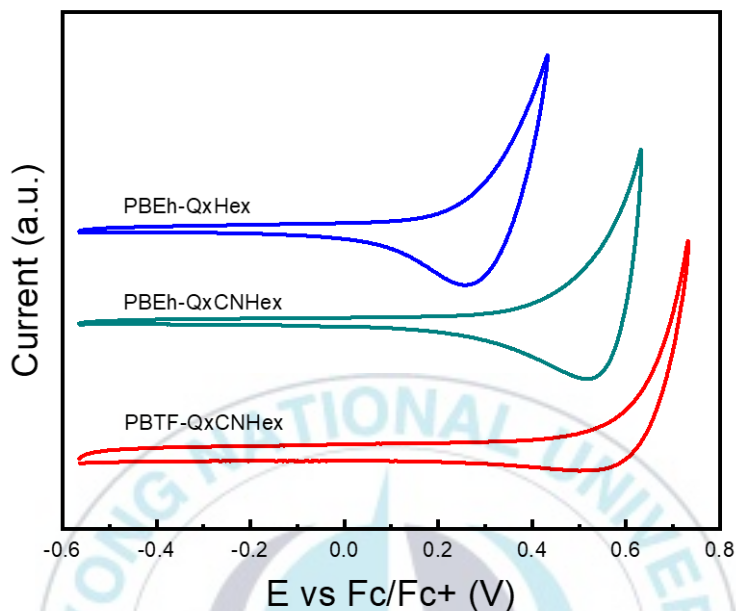


**Figure III-3.** Cyclic voltammograms of polymers

To understand the significant relation from optical to electrochemical properties, the cyclic voltammograms (CVs) analysis were carried out to measure the oxidation onset potential using 4.8 eV of ferrocene energy level as the standard under vacuum condition, which then can be used to calculate HOMO energy levels of all polymers with the curve is illustrated in **Figure III-3**. As summarized in **Table III-2**, the HOMO level of **PBEh-QxHex**, **PBEh-QxCNHex**, and **PBTF-QxCNHex** are -5.04, -5.17, and -5.25, respectively. Related to the trend on the optical band gap, by adding a cyano group on the acceptor unit of **PBEh-QxCNHex**,

the HOMO energy level can be decreased owing to an increase in electron affinity as a result of stronger electronegativity of cyano substituent [34,35,37,44]. In addition, the combination of cyanated-quinoxaline with fluorinated-BDT donor also lead to deeper HOMO level of **PBTF-QxCNHex** due to strong electron-withdrawing effect from fluorine moiety [40,45–47].

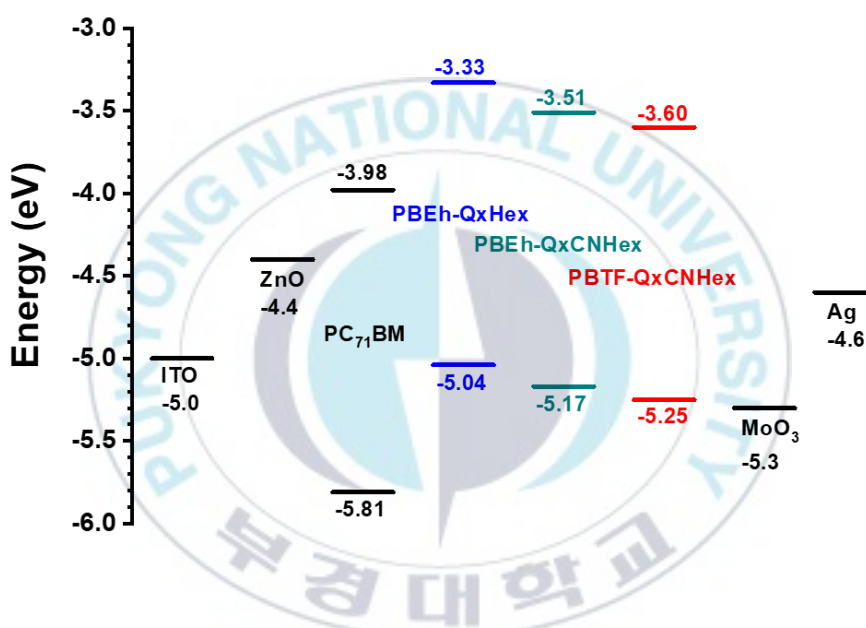


**Figure III-4.** Energy level diagram of all materials used in the inverted type PSCs device

Moreover, the LUMO energy levels of all-three polymers were determined from calculation between the HOMO energy levels and the optical band gaps, which are -3.33, -3.51, and -3.60, respectively. As a result from CV data, the summary of energy levels diagram of the polymers, PC<sub>71</sub>BM and the other materials used in device fabricated are shown in **Figure III-4**. The overall results based on

CV and UV-Vis analysis can be summarized that introducing strong electron-withdrawing like cyano group and the combination with fluorine moiety in alkylthienyl substituent of donor unit can give significant effect to all polymers for possessing lower band gap to absorb more photon effectively.

### III-3. Theoretical Calculations of Polymers

The frontier molecular orbitals of all-polymers to know the theoretical electronic properties was investigated using the density functional theory (DFT) of the Gaussian 09 program at the B3LYP/6-31G\*\* level. The computational calculation was simplified by changing all the hexyl and ethyl hexyl side chains on the DPQ acceptor and the BDT donor, respectively, to be methyl groups and the two repeating units are represented the long polymer chains. As displayed in **Figure III-5**, the delocalization of the HOMO wave functions of the polymers occurs along their BDT backbones meanwhile, mostly localization of the LUMO wave functions takes place in the electron-withdrawing DPQ units. The result of the calculation states that the introduction of a cyano group into the quinoxaline can decrease the LUMO significantly, but reduce the HOMO slightly. Moreover, the orthogonality between HOMO and LUMO of the cyanated polymers is also increased due to the strong charge-transfer interaction from the cyano group, which can be seen from a change of the dihedral angle between the thiophene bridge and the DPQ monomer of cyanated polymers ( $41.86^\circ$  and  $42.18^\circ$  for **PBEh-QxCNHex** and **PBTF-QxCNHex**, respectively) from non-cyanated polymer ( $25.47^\circ$  for **PBEh-QxHex**).

Besides, the substitution of fluorothiophene on the BDT unit leads to a further reduction of both the HOMO and LUMO energy levels. Those prove that the HOMO and LUMO energy levels trends from the theoretical calculation well resemble with the experimental results.

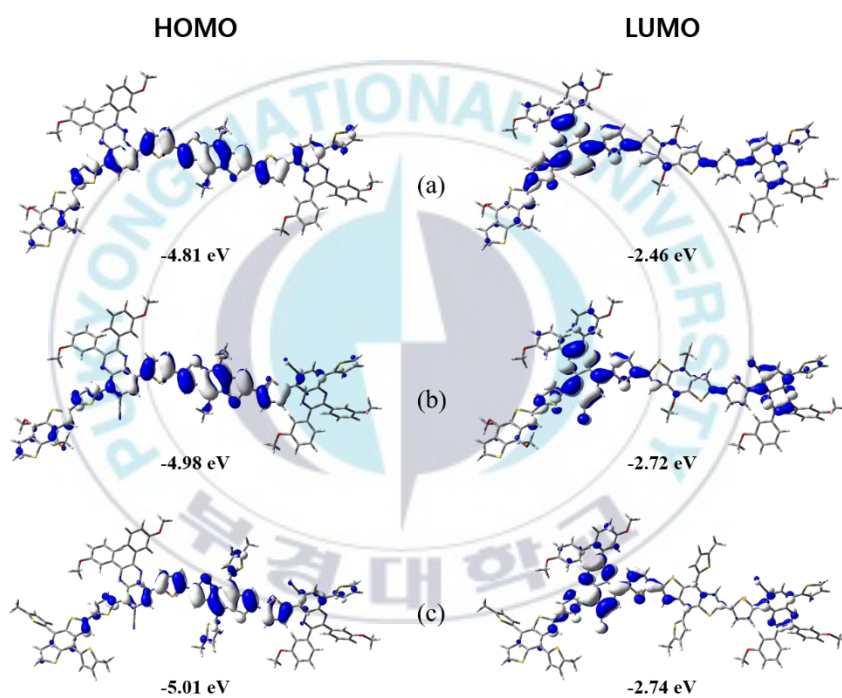


**Figure III-5.** Frontier molecular orbitals of two-repeating unit models with HOMO and LUMO energy levels calculated at the B3LYP/6-31G\*\* level for (a) PBEh-QxHex, (b) PBEh-QxCNHex, and (c) PBTF-QxCNHex

### III-4. Photovoltaic Properties of Polymers

The inverted-type of polymer solar cells device with the structure of indium tin oxide (ITO) (15 $\Omega$ )/ZnO (25 nm)/active layer (donor polymer: PC<sub>71</sub>BM) (95 nm)/MoO<sub>3</sub> (3 nm)/Ag (100 nm) were fabricated to explain the photovoltaic properties of these three polymers.

**Table III-3.** The best photovoltaic parameters of the PSCs. The averages for the photovoltaic parameters of each device are given in parentheses.

Polymer	$J_{sc}$ (mA/cm <sup>2</sup> )	$V_{oc}$ (V)	FF (%)	PCE (%)	$R_s$ ( $\Omega$ cm <sup>2</sup> ) <sup>a</sup>
<b>PBEh-QxHex</b>	13.94 (13.74)	0.62 (0.62)	58.4 (58.4)	5.05 (4.97)	2.89
<b>PBEh-QxCNHex</b>	17.24 (16.60)	0.79 (0.79)	53.3 (52.0)	7.26 (6.80)	3.09
<b>PBTF-QxCNHex</b>	15.59 (15.50)	0.92 (0.92)	60.7 (60.4)	8.66 (8.61)	2.71

<sup>a</sup>Series resistance estimated from the corresponding best device.

The active layer condition for device analysis used various blend ratio of donor polymer ranging from 3:3 to 3:6 w/w in chlorobenzene, which to be found that the optimum blend ratios of **PBEh-QxHex**, **PBEh-QxCNHex**, and **PBTF-QxCNHex** to PC<sub>71</sub>BM were obtained to be 3:4, 3:4, and 3:5, respectively with 3% v/v of 1,8-diiodooctane (DIO) as the additive for processing. The energy level diagram as

illustrated in **Figure III-4** is demonstrated an efficient charge separation from the blend films and so do charge carrier transport process in polymer solar cells, which can be seen that the difference of LUMO energy level between all donor polymers to PC<sub>71</sub>BM is over 0.3 eV and imply that all these polymers have a favorable downhill driving force to separate the exciton efficiently.

The current density-voltage (*J-V*) curves at the optimum blend ratio condition for all polymers under 1.0 sun condition (inset: the curves found under dark conditions) are displayed in **Figure III-6a**, and the parameter data are summarized in **Table III-3**. Interestingly, the PCEs of the device polymers, with **PBEh-QxHex** as the reference, have a considerable improvement in the order **PBEh-QxCNHex** and **PBTF-QxCN** from 5.05% to be 7.26%, and then more increase to be 8.66%, which have a correlation with the increasing of  $V_{oc}$  value of the device of these polymers. The  $V_{oc}$  values of the **PBEh-QxHex**, **PBEh-QxCNHex**, and **PBTF-QxCNHex** are 0.62 V, 0.79 V, and 0.92 V, respectively. These step-by-step enhancements in  $V_{oc}$  value are related to the decrease of HOMO energy levels to lower value along with the incorporation of the strong electron-

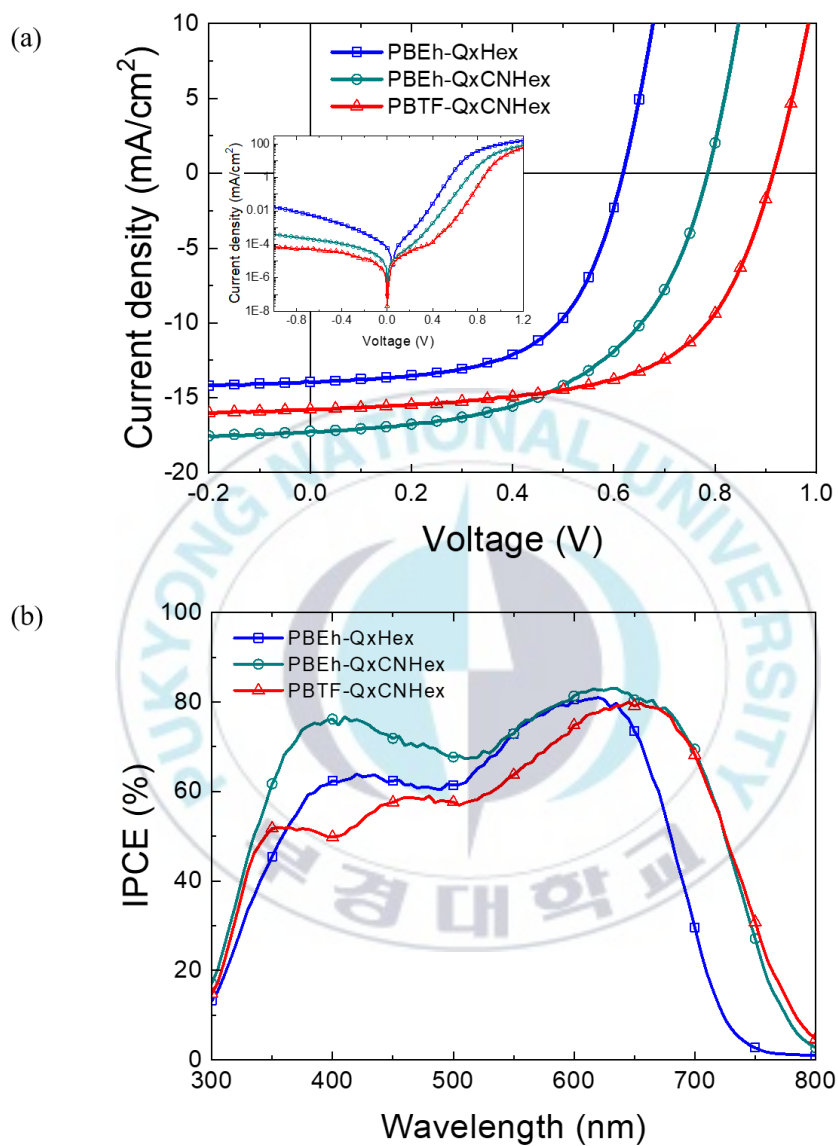


**Figure III-6.** (a) Current density vs. voltage curves of PSCs with optimum blend ratio of polymer donor to PC<sub>71</sub>BM under 1.0 sun condition (inset: under dark condition) and (b) IPCE spectra of PSCs based on **PBEh-QxHex**, **PBEh-QxCNHex**, and **PBTF-QxCNHex**.

withdrawing moiety, both on acceptor and donor unit. Concerning this result, some previous result also reported the effect of cyano group and fluorine atom to the rising of  $V_{oc}$  value at the same of D-A type structure [35,40,44,45].

Moreover, as noticed in **Table III-3**, the  $J_{sc}$  values of both **PBEh-QxCNHex** (17.24 mA/cm<sup>2</sup>) and **PBTF-QxCNHex** (15.59 mA/cm<sup>2</sup>) show a higher value than **PBEh-QxHex** (13.94 mA/cm<sup>2</sup>). The cyanated-polymer, which result in the lower bandgap of polymer, possess broader of absorption spectra and allow a large amount of exciton to be generated in the film, and so leads to increase  $J_{sc}$  value [34,48]. Unfortunately, the  $J_{sc}$  value of the device based on **PBTF-QxCNHex** is lower than from the device based on **PBEh-QxCNHex**. The decreasing of  $J_{sc}$  value might have occurred due to this polymer has a lower power to absorb the light for generating the exciton. This can be caused by a smaller molar extinction coefficient of **PBTF-QxCNHex** ( $4.61 \times 10^4 \text{ M}^{-1} \text{ cm}^{-1}$ ) than **PBEh-QxCNHex** ( $5.00 \times 10^4 \text{ M}^{-1} \text{ cm}^{-1}$ ) which is illustrated in the incident photon-to-current efficiency (IPCE) curve in **Figure III-6b**, since **PBTF-QxCNHex** having lower molecular weight than **PBEh-QxCNHex**, as a result of the substitution of BDT-alkoxy to BDT-alkylthienyl. Meanwhile, the best value of fill factor ( $FF$ ) is achieved by the device based on **PBTF-QxCNHex** at 60.7% as consistent with the highest of PCE, while the other devices based on **PBEh-QxHex** and **PBEh-QxCNHex** are obtained 58.4% and 53.3%, respectively.

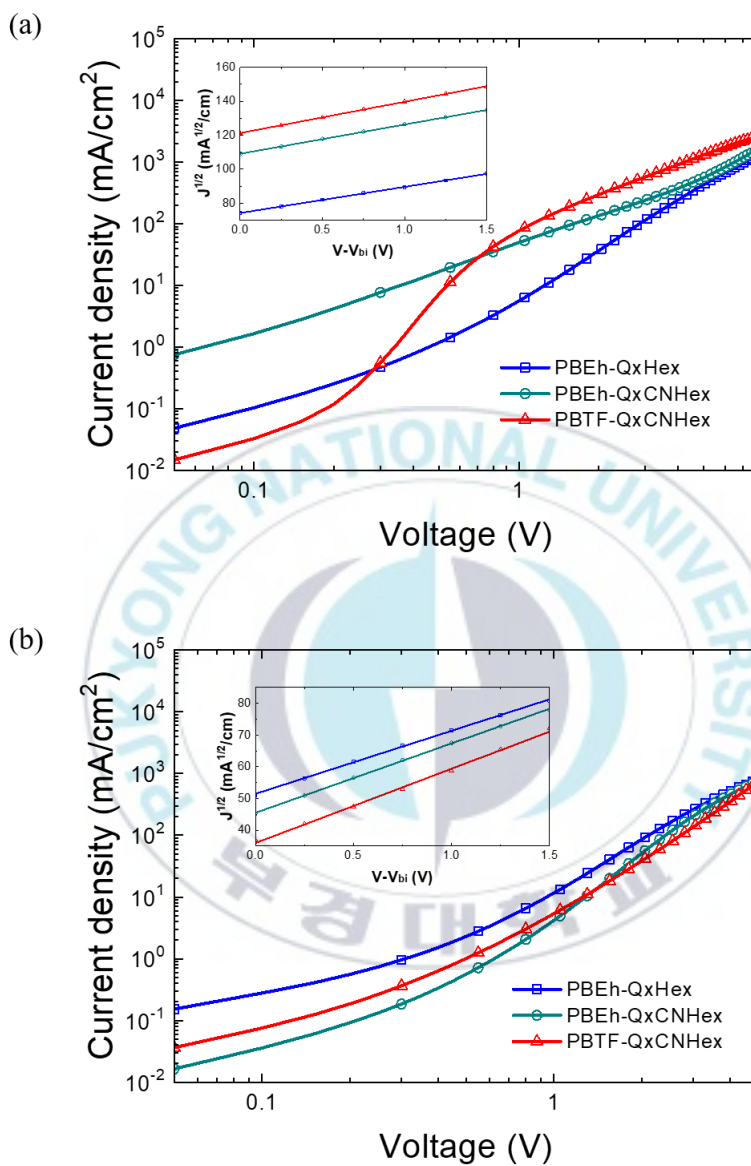


**Figure III-7.** Current density vs. voltage curves of (a) hole-only and (b) electron-only devices based on **PBEh-QxHex**, **PBEh-QxCNHex**, and **PBTF-QxCNHex** including the inset showing current density vs. voltage (V) –built-in voltage ( $V_{bi}$ ) with fitted lines.

Then, based on the IPCE curve in **Figure III-6b**, all the polymers are in good agreement with the trend in  $J_{sc}$  values and they show very good absorption in the broadening range of 300-800 nm. It also obtains that the cyanated-polymer show broader absorption spectra compare than without a cyano group. In addition, the series resistance ( $R_s$ ) of the device based **PBTF-QxCNHex** achieve the smallest value of  $2.71 \Omega \text{ cm}^2$  than those devices based on **PBEh-QxHex** ( $2.89 \Omega \text{ cm}^2$ ) and **PBEh-QxCNHex** ( $3.09 \Omega \text{ cm}^2$ ) as shown in **Table III-3**. This is well consistent with the photovoltaic properties of the devices and exhibits the incorporation a number of the electron-withdrawing group on to polymer backbone can reduce the  $R_s$  value gradually [30,43].

On the other hand, to elucidate the behavior of charging transporting properties of the polymers, electron- and hole-only devices were fabricated according to the structure of ITO ( $15 \Omega$ )/ZnO (25nm)/donor polymer: PC<sub>71</sub>BM (95nm)/LiF (1nm)/Al (100nm) and ITO ( $15 \Omega$ )/PEDOT: PSS (40 nm)/donor polymer: PC<sub>71</sub>BM (95nm)/Au (50 nm), respectively. These mobility behaviors were calculated by space charge limited current (SCLC) measurement which the characteristics are shown in **Figure III-7a,b** and correspond on to renowned Mott-Gurney law [49]. The hole mobility of the device based on **PBTF-QxCNHex** exhibits the highest at  $7.48 \times 10^{-3} \text{ cm}^2 \text{ V}^{-1} \text{ s}^{-1}$  compare than **PBEh-QxCNHex** ( $6.52 \times 10^{-3} \text{ cm}^2 \text{ V}^{-1} \text{ s}^{-1}$ ) and **PBEh-QxHex** ( $5.21 \times 10^{-3} \text{ cm}^2 \text{ V}^{-1} \text{ s}^{-1}$ ). Similarly, the electron mobility of the devices fabricated with **PBEh-QxHex**, **PBEh-QxCNHex**, and

**PBTF-QxCNHex** are  $6.25 \times 10^{-3}$ ,  $7.57 \times 10^{-3}$ , and  $8.68 \times 10^{-3} \text{ cm}^2 \text{ V}^{-1}\text{s}^{-1}$ , respectively. It can be seen that the adding of some electron-withdrawing substituents like cyano and fluorine atoms can enhance the hole and electron mobilities, which are well-agreed with better performance of the device based on **PBTF-QxCNHex** [34,40,48].

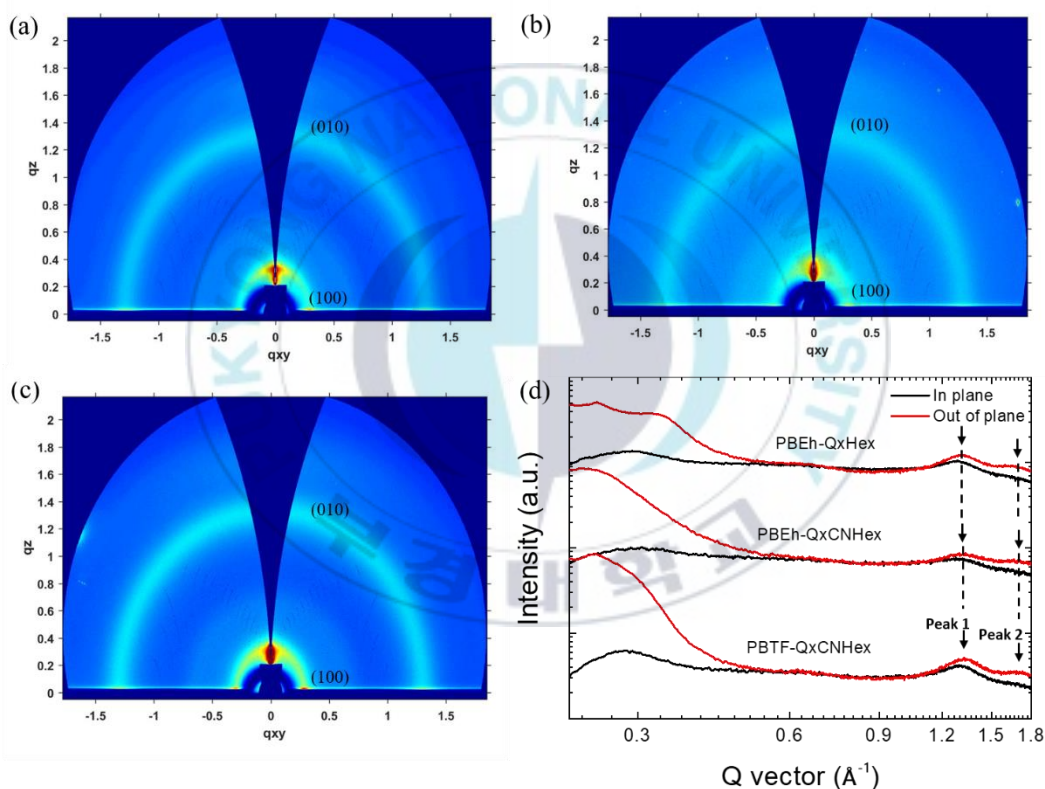


**Figure III-8.** GIWAXS patterns of the blend films of (a) **PBEh-QxHex**, (b) **PBEh-QxCNHex**, and (c) **PBTF-QxCNHex** with PC<sub>71</sub>BM in 2D, and (d) their corresponding in 1D profiles along the in-plane and out-of-plane intensity.

In order to investigate the molecular orientation and stacking of all-donor polymer films in the blend with PC<sub>71</sub>BM, the GIWAXS measurement has been done and the results are shown in **Figure III-8**. As displayed in the two-dimensional (2D) pattern of GIWAXS in **Figure III-8(a-c)**, a strong  $\pi$ - $\pi$  stacking diffraction peak at (010) position in  $q_z$  demonstrate the out-of-plane direction, while strong lamellar stacking diffraction peak at (100) position in  $q_{xy}$  illustrate in-plane direction. These reflection patterns indicated that all-polymer films have the face-on orientation [17,50] which was also observed from no peak observed in the in-plane direction for all polymer films (peak 2) in the 1D profile of pattern, as shown in **Figure III-8d**. The face-on orientation is considered as the favorable molecular ordering for organic solar cells because the polymer-film is placed facing to the substrate which means the  $\pi$ - $\pi$  stacking is in the normal film direction. It would allow the charges to move along the out-of-plane direction, so the charge mobility could increase, leading to improve the device performance of solar cells [51,52].

More information about  $\pi$ - $\pi$  stacking peak of all-polymer film is given in the 1D profile in **Figure III-8d**. From that curve, peak 1 corresponded to PC<sub>71</sub>BM meanwhile peak 2 correlated to polymer films. It can be seen that PC<sub>71</sub>BM show  $\pi$ - $\pi$  stacking peak in both out-of-plane and in-plane directions, but on the other hand, all-polymer films only show  $\pi$ - $\pi$  stacking peak in the out-of-plane as mention previously. The **PBEh-QxHex** exhibit  $\pi$ - $\pi$  stacking peak at  $1.63 \text{ \AA}^{-1}$  (d-spacing:  $3.86 \text{ \AA}$ ), while **PBEh-QxCNHex** and **PBTF-QxCNHex** show the higher value of

$\pi$ - $\pi$  stacking peak at  $1.65 \text{ \AA}^{-1}$  (d-spacing:  $3.80 \text{ \AA}$ ) and  $1.64 \text{ \AA}^{-1}$  (d-spacing:  $3.83 \text{ \AA}$ ), respectively. The smaller d-spacing of two cyanated-polymers reveals that they have stronger intermolecular interaction than the polymer without a cyano substituent [53,54], which then results in enhanced device performance.

Furthermore, the morphologies of the **PBEh-QxHex**, **PBEh-QxCNHex**, and **PBTF-QxCNHex** films in blending with PC<sub>71</sub>BM were represented in transmission electron microscopy (TEM) image in 200 nm of scale bar as shown in **Figure III-9**. All of the polymers exhibit uniform morphologies with no aggregation, which mean they are well-mixed to PC<sub>71</sub>BM. Interestingly, by the incorporation of the cyano group, the blend films of **PBEh-QxCNHex** and **PBTF-QxCNHex** show smaller domain size than **PBEh-QxHex**. The smaller domain size can give more effective charge carrier transportation to enhance performance of polymer solar cells. However, the **PBEh-QxCNHex** domain does not have fibrillar structure like **PBEh-QxHex** and **PBTF-QxCNHex** which allow the holes and electrons non-geminate recombination to occur in the device performance and result in lower *FF* value.

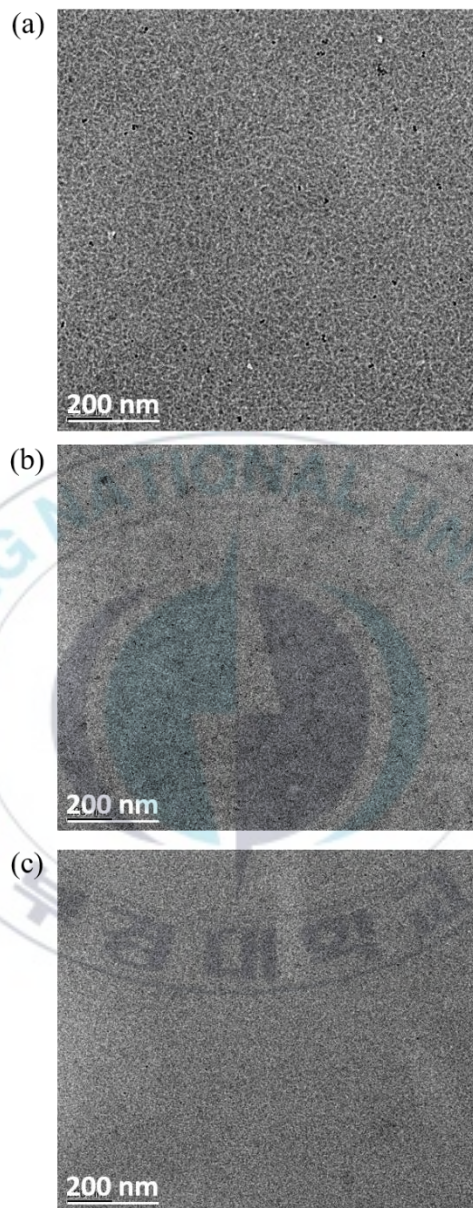
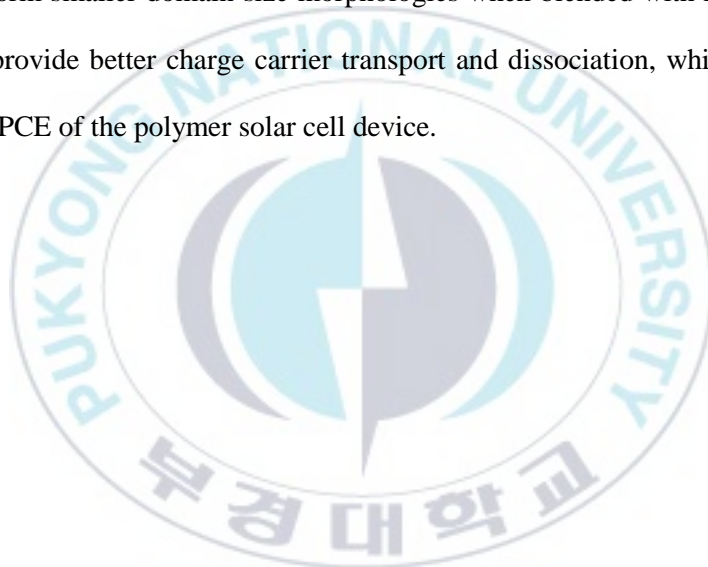


**Figure III-9.** TEM images of the blend films of (a) **PBEh-QxHex**, (b) **PBEh-QxCNHex**, and (c) **PBTF-QxCNHex** with PC<sub>71</sub>BM in 200 nm of scale bar.

In addition, **PBTF-QxCNHex** exhibits an increased phase separation with small fiber structure comparing to **PBEh-QxCNHex** since the crystallinity degree of **PBTF-QxCNHex** is higher than **PBEh-QxCNHex**, as shown in **Figure III-8d** due to the incorporation of fluorine atoms on alkylthienyl which replace the alkoxy substituent on the BDT structure [40,45,47]. Overall, the introduction of the cyano group on the acceptor unit and fluorine atoms on the donor unit can lead to forming more uniform smaller domain size morphologies when blended with PC<sub>71</sub>BM, so they can provide better charge carrier transport and dissociation, which result in improved PCE of the polymer solar cell device.



## Chapter IV. Conclusion

Three new conjugated polymers have been synthesized by using the Stille coupling reaction. The Benzodithiophene (BDT) with alkoxy side chain as the electron-donating connected to diphenylquinoxaline (DPQ) derivatives with hexyl side chain in *meta* position of the phenyl rings as the electron-accepting through a thiophene bridge denoted as **PBEh-QxHex**. A cyano group as the active electron-withdrawing substituent was introduced on the 6,7-position of DPQ to form **PBEh-QxCNHex**. Besides, a substitution of 2-ethylhexyloxy to 2-ethylhexyl fluorinated-thiophene groups on BDT unit afforded **PBTF-QxCNHex**. The result from photovoltaic properties demonstrates the PCE in order **PBEh-QxHex** (5.05%), **PBEh-QxCNHex** (7.26%), and **PBTF-QxCNHex** (8.66%). The enhancement of PCE relates to the incorporation of the cyano group on the DPQ unit and fluorine atoms on the BDT-alkylthienyl unit. These incorporations gave beneficial impacts such as the significant reduction of HOMO energy level leading to the increase of  $V_{oc}$  value and improved the charge carrier mobility owing to better morphology in the active layer of the device, results in higher  $J_{sc}$  value. The introducing of alkylthienyl in order to replace alkoxy moiety also contributes to developing better intermolecular planarity, which induces excellent carrier mobility and so affords in enhancing  $FF$  value. However, the transition of planarity on the polymer backbone from **PBEh-QxCNHex** to **PBTF-QxCNHex** gives changes in the morphology structure and the molar extinction coefficient which causes a

decrease of  $J_{sc}$  value. Therefore, this study can provide a further understanding of the incorporation effect of the electron-withdrawing substituent, such as a cyano group and fluorine atoms, on the conjugated polymer which have D-A structure type. Furthermore, the optimization study for better morphology of blends film based on the cyanated-conjugated polymers still needed to improve the device performance for supporting their promising advantages in the photovoltaic cell application.



## References

- [1] Fabiani Appavou, Adam Brown, Bärbel Epp, Duncan Gibb, Bozhil Kondev, Angus McCrone, Hannah E. Murdock, Evan Musolino, Lea Ranalder, Janet L. Sawin, Kristin Seyboth, Jonathan Skeen, F.S. (2019) Renewables in Cities - 2019 Global Status Report. .
- [2] Parida, B., Iniyar, S., and Goic, R. (2011) A review of solar photovoltaic technologies. *Renewable and Sustainable Energy Reviews*. 15 (3), 1625–1636.
- [3] (2019) NREL Best Research-Cell Efficiencies. <https://www.nrel.gov/pv/assets/pdfs/best-research-cell-efficiencies.20190802.pdf>
- [4] Sinke, W.C. (2019) Development of photovoltaic technologies for global impact. *Renewable Energy*. 138 911–914.
- [5] Battersby, S. (2019) News Feature: The solar cell of the future. *Proceedings of the National Academy of Sciences of the United States of America*. 116 (1), 7–10.
- [6] Inganäs, O. (2018) Organic Photovoltaics over Three Decades. *Advanced Materials*. 30 (35), 1–26.
- [7] Zhao, J., Li, Y., Yang, G., Jiang, K., Lin, H., Ade, H., et al. (2016) Efficient organic solar cells processed from hydrocarbon solvents. *Nature Energy*. 1 (2),.
- [8] Cui, Y., Yao, H., Zhang, J., Zhang, T., Wang, Y., Hong, L., et al. (2019) Over 16% efficiency organic photovoltaic cells enabled by a chlorinated acceptor with increased open-circuit voltages. *Nature Communications*. 10 (1), 1–8.
- [9] Rafique, S., Abdullah, S.M., Sulaiman, K., and Iwamoto, M. (2018) Fundamentals of bulk heterojunction organic solar cells: An overview of

- stability/degradation issues and strategies for improvement. *Renewable and Sustainable Energy Reviews*. 84, 43–53.
- [10] Arbouch, I., Karzazi, Y., and Hammouti, B. (2014) Organic photovoltaic cells: Operating principles, recent developments and current challenges – review. *Physical and Chemical News*. 72 (4), 73–84.
- [11] Nicholson, P.G. and Castro, F.A. (2010) Organic photovoltaics: Principles and techniques for nanometre scale characterization. *Nanotechnology*. 21 (49),.
- [12] Agrawal, G.D. and A, V.K. (2014) Organic Solar Cells: Principles, Mechanism and Recent Developments. *International Journal of Research in Engineering and Technology*. 03 (09), 338–341.
- [13] Jørgensen, M., Norrman, K., Gevorgyan, S.A., Tromholt, T., Andreasen, B., and Krebs, F.C. (2012) Stability of polymer solar cells. *Advanced Materials*. 24 (5), 580–612.
- [14] Ganesamoorthy, R., Sathiyam, G., and Sakthivel, P. (2017) Review: Fullerene based acceptors for efficient bulk heterojunction organic solar cell applications. *Solar Energy Materials and Solar Cells*. 161, 102–148.
- [15] Wang, T., Sun, R., Xu, S., Guo, J., Wang, W., Guo, J., et al. (2019) A wide-bandgap D-A copolymer donor based on a chlorine substituted acceptor unit for high performance polymer solar cells. *Journal of Materials Chemistry A*. 7 (23), 14070–14078.
- [16] Rand, B.P. and Richter, H. (2014) Organic Solar Cells: Fundamentals, Devices, and Upscaling. Jenny Stanford Publishing, .
- [17] Huang, Y., Kramer, E.J., Heeger, A.J., and Bazan, G.C. (2014) Bulk heterojunction solar cells: Morphology and performance relationships. *Chemical Reviews*. 114 (14), 7006–7043.
- [18] Lalevée, J. and Fouassier, J.P. (2015) Dyes and chromophores in polymer science.

- [19] Dennler, B.G., Scharber, M.C., and Brabec, C.J. (2015) Polymer-Fullerene Bulk-Heterojunction Solar Cells. *Advanced Materials*. 21 1323–1338.
- [20] Brus, V. V., Lee, J., Luginbuhl, B., Ko, S.J., Bazan, G.C., and Nguyen, T.Q. (2019) Solution-Processed Semitransparent Organic Photovoltaics: From Molecular Design to Device Performance. *Advanced Materials*. 1900904 1–26.
- [21] Jung, J.W., Jo, J.W., Jung, E.H., and Jo, W.H. (2016) Recent progress in high efficiency polymer solar cells by rational design and energy level tuning of low bandgap copolymers with various electron-withdrawing units. *Organic Electronics: Physics, Materials, Applications*. 31 149–170.
- [22] Yao, H., Ye, L., Zhang, H., Li, S., Zhang, S., and Hou, J. (2016) Molecular design of benzodithiophene-based organic photovoltaic materials. *Chemical Reviews*. 116 (12), 7397–7457.
- [23] Bang, S.M., Park, J. hyun, Kang, S., Lee, Y.S., Lim, B., Heo, H., et al. (2017) Thienopyrroledione and benzodithiophene/thiophene-based random terpolymer for polymer solar cells with improved fill factor. *Dyes and Pigments*. 140 229–235.
- [24] Gedefaw, D., Tessarolo, M., Bolognesi, M., Prosa, M., Kroon, R., Zhuang, W., et al. (2016) Synthesis and characterization of benzodithiophene and benzotriazole-based polymers for photovoltaic applications. *Beilstein Journal of Organic Chemistry*. 12 1629–1637.
- [25] Duan, R., Ye, L., Guo, X., Huang, Y., Wang, P., Zhang, S., et al. (2012) Application of two-dimensional conjugated benzo[1,2-b:4,5-b']dithiophene in quinoxaline-based photovoltaic polymers. *Macromolecules*. 45 (7), 3032–3038.
- [26] Yu, T., Xu, X., Zhang, G., Wan, J., Li, Y., and Peng, Q. (2017) Wide Bandgap Copolymers Based on Quinoxalino[6,5-f].quinoxaline for Highly Efficient Nonfullerene Polymer Solar Cells. *Advanced Functional*

*Materials*. 27 (28), 1–11.

- [27] Song, K.W., Lee, T.H., Ko, E.J., Back, K.H., and Moon, D.K. (2014) Polymer solar cells based on quinoxaline and dialkylthienyl substituted benzodithiophene with enhanced open circuit voltage. *Journal of Polymer Science, Part A: Polymer Chemistry*. 52 (7), 1028–1036.
- [28] Gedefaw, D., Prosa, M., Bolognesi, M., Seri, M., and Andersson, M.R. (2017) Recent Development of Quinoxaline Based Polymers/Small Molecules for Organic Photovoltaics. *Advanced Energy Materials*. 7 (21), 1–38.
- [29] Putri, S.K., Kim, Y.H., Whang, D.R., Kim, J.H., and Chang, D.W. (2018) Synthesis of Trifluoromethylated Quinoxaline-Based Polymers for Photovoltaic Applications. *Macromolecular Rapid Communications*. 39 (16), 1–7.
- [30] Kurnia, S., Hwan, Y., Ryeol, D., Seok, M., Hyun, J., and Wook, D. (2017) Step-by-step improvement in photovoltaic properties of fluorinated quinoxaline-based low-band-gap polymers. *Organic Electronics*. 47 14–23.
- [31] Hwang, K.H., Kim, D.H., Choi, M.H., Han, J.P., and Moon, D.K. (2016) Effect of side chain position and conformation of quinacridone-quinoxaline based conjugated polymers on photovoltaic properties. *Journal of Industrial and Engineering Chemistry*. 34 66–75.
- [32] Huang, Y., Huo, L., Zhang, S., Guo, X., Han, C.C., Li, Y., et al. (2011) Sulfonyl: A new application of electron-withdrawing substituent in highly efficient photovoltaic polymer. *Chemical Communications*. 47 (31), 8904–8906.
- [33] Hu, Z., Chen, H., Qu, J., Zhong, X., Chao, P., Xie, M., et al. (2017) Design and Synthesis of Chlorinated Benzothiadiazole-Based Polymers for Efficient Solar Energy Conversion. *ACS Energy Letters*. 2 (4), 753–758.
- [34] Casey, A., Dimitrov, S.D., Shakya-Tuladhar, P., Fei, Z., Nguyen, M., Han,

- Y., et al. (2016) Effect of Systematically Tuning Conjugated Donor Polymer Lowest Unoccupied Molecular Orbital Levels via Cyano Substitution on Organic Photovoltaic Device Performance. *Chemistry of Materials*. 28 (14), 5110–5120.
- [35] Cha, H., Kim, H.N., An, T.K., Kang, M.S., Kwon, S.K., Kim, Y.H., et al. (2014) Effects of cyano-substituents on the molecular packing structures of conjugated polymers for bulk-heterojunction solar cells. *ACS Applied Materials and Interfaces*. 6 (18), 15774–15782.
- [36] Casey, A., Green, J.P., Shakya Tuladhar, P., Kirkus, M., Han, Y., Anthopoulos, T.D., et al. (2017) Cyano substituted benzotriazole based polymers for use in organic solar cells. *Journal of Materials Chemistry A*. 5 (14), 6465–6470.
- [37] Lu, J., Yuan, J., Guo, W., Huang, X., Liu, Z., Zhao, H., et al. (2014) Effects of cyano (CN)-groups on the planarity, film morphology and photovoltaic performance of benzodithiophene-based polymers. *Polymer Chemistry*. 5 (16), 4772–4780.
- [38] Yang, M.H., Jin, H.C., Kim, J.H., and Chang, D.W. (2019) Synthesis of cyano-substituted conjugated polymers for photovoltaic applications. *Polymers*. 11 (5), 1–13.
- [39] Zhang, Q., Kelly, M.A., Bauer, N., and You, W. (2017) The Curious Case of Fluorination of Conjugated Polymers for Solar Cells. *Accounts of Chemical Research*. 50 (9), 2401–2409.
- [40] Abdulahi, B.A., Li, X., Mone, M., Kiros, B., Genene, Z., Qiao, S., et al. (2019) Structural Engineering of Pyrrolo[3,4-f]benzotriazole-5,7(2H,6H)-dione-based Polymers for Non-fullerene Organic Solar Cells with an Efficiency over 12%. *Journal of Materials Chemistry A*. 19522–19530.
- [41] Liu, H.Y., Wu, P.J., Kuo, S.Y., Chen, C.P., Chang, E.H., Wu, C.Y., et al. (2015) Quinoxaline-based polymer dots with ultrabright red to near-infrared

- fluorescence for in vivo biological imaging. *Journal of the American Chemical Society*. 137 (32), 10420–10429.
- [42] Liao, L., Dai, L., Smith, A., Durstock, M., Lu, J., Ding, J., et al. (2007) Photovoltaic-active dithienosilole-containing polymers. *Macromolecules*. 40 (26), 9406–9412.
- [43] Putri, S.K., Jin, H.C., Whang, D.R., Kim, J.H., and Chang, D.W. (2019) Enhanced open-circuit voltages of trifluoromethylated quinoxaline-based polymer solar cells. *Organic Electronics: Physics, Materials, Applications*. 65 363–369.
- [44] Casey, A., Han, Y., Fei, Z., White, A.J.P., Anthopoulos, T.D., and Heaney, M. (2015) Cyano substituted benzothiadiazole: A novel acceptor inducing n-type behaviour in conjugated polymers. *Journal of Materials Chemistry C*. 3 (2), 265–275.
- [45] Liu, D., Zhao, W., Zhang, S., Ye, L., Zheng, Z., Cui, Y., et al. (2015) Highly Efficient Photovoltaic Polymers Based on Benzodithiophene and Quinoxaline with Deeper HOMO Levels. *Macromolecules*. 48 (15), 5172–5178.
- [46] Zhao, W., Li, S., Yao, H., Zhang, S., Zhang, Y., Yang, B., et al. (2017) Molecular Optimization Enables over 13% Efficiency in Organic Solar Cells. *Journal of the American Chemical Society*. 139 (21), 7148–7151.
- [47] Zhang, M., Guo, X., Zhang, S., and Hou, J. (2014) Synergistic effect of fluorination on molecular energy level modulation in highly efficient photovoltaic polymers. *Advanced Materials*. 26 (7), 1118–1123.
- [48] Feng, K., Xu, X., Li, Z., Li, Y., Li, K., Yu, T., et al. (2015) Low band gap benzothienophene - Thienothiophene copolymers with conjugated alkylthiothieryl and alkoxy carbonyl cyanovinyl side chains for photovoltaic applications. *Chemical Communications*. 51 (29), 6290–6292.
- [49] Bagui, A. and Iyer, S.S.K. (2014) Increase in hole mobility in poly (3-

hexylthiophene-2,5-diyl) films annealed under electric field during the solvent drying step. *Organic Electronics: Physics, Materials, Applications*. 15 (7), 1387–1395.

- [50] Su, Y.W., Lin, Y.C., and Wei, K.H. (2017) Evolving molecular architectures of donor-acceptor conjugated polymers for photovoltaic applications: From one-dimensional to branched to two-dimensional structures. *Journal of Materials Chemistry A*. 5 (46), 24051–24075.
- [51] Mo, D., Wang, H., Chen, H., Qu, S., Chao, P., Yang, Z., et al. (2017) Chlorination of Low-Band-Gap Polymers: Toward High-Performance Polymer Solar Cells. *Chemistry of Materials*. 29 (7), 2819–2830.
- [52] Applications, I. (2015) Enhancement of out-of-plane mobility in P3HT film : Face-on orientation produced by rubbing. 116–117.
- [53] Qiu, B., Chen, S., Xue, L., Sun, C., Li, X., Zhang, Z.G., et al. (2018) Effects of alkoxy and fluorine atom substitution of donor molecules on the morphology and photovoltaic performance of all small molecule organic solar cells. *Frontiers in Chemistry*. 6, 1–9.
- [54] Lee, T.H., Choi, M.H., Jeon, S.J., Nam, S.J., Han, Y.W., Haw, J.R., et al. (2017) Improvement of short circuit current density by intermolecular interaction between polymer backbones for polymer solar cells. *Polymer Journal*. 49 (1), 177–187.

## Acknowledgements

First of all, I give my most enormous gratitude to Jesus Christ for all His blessing, guidance, promise, and strength for me in every condition I have been through during my master studies in Korea until today.

My best appreciation then is presented to my advisor, Prof. Dong Wook Chang, for his kind-hearted support and supervision to me, encouraging me to be a good researcher for my future. I also express my thanks to Prof. Joo Hyun Kim and Hocheol, who help me in the solar cell device work, and so Prof. Min Young Shon and Prof. Young Eup Jin, as well as the officers in the Department of Industrial Chemistry who always help me. And my best gratitude is given to all my labmates: Shinta, Munho, Juntae, Ratri, and Seokwoo for our teamwork, giving me the best advice, helping and cheering up me. Also, to Mba Sella, an alumnus of this lab, for encouraging me to pursue one of my dreams come true here.

My deep gratefulness goes to my parents, Ariesta, and Timoty in Indonesia, Mas Limpat, and also to my best friends in Indonesia: Oca, Irma Mei, Mas Fanny, and Ventie for the love, the prayers, the cheers, and their best advices during my living far away here. And to my Sooyoungro Indonesia Service family here: Pak Nanang, Bu Ester, Pak Jotje, Kak Febrina, Raquel, Eunice and Ko Endro-Ci Maria, thanks to our fellowship and God's service time together, full of good memories.

Thanks to my friends here in Engineering building: Merreta, Mba Intan, and Mas Arda, who two-years struggle together, also Mba Sabrina, Mba Ratna, Mba Moli, Mba Puji, and Ace for laughing together in the middle of our busy times.

“I thank my God everytime I remember you.” – Phillipians 1: 3

Pukyong National University Busan, South Korea

January 2020

Christyowati Primi Sagita